Master thesis in Materials, energy and nanotechnology

Ole Joachim Svendsen

Down shifting of light with thin films

Magnitude: 60 study points

DEPARTMENT OF CHEMESTRY/PHYSICS
The Faculty of Mathematics and Natural Sciences
UNIVERSITY OF OSLO

March 3, 2014

Foreword

This work in this thesis has been performed in the Center for Materials Science and Nanotechnology (SMN) in the Chemistry department at the University of Oslo. The thesis work was started in January of 2012 and ended in March of 2014.

Thanks and all honors are due to thesis supervisor Ola Nilsen and co-supervisor Per-Anders Hansen for their aid and support throughout the project. Additional thanks go to the Department of Geosciences, UiO, for use of the XRF equipment. Thanks also go to Chris Ian Thomas for aid in using the H_2 furnace and equipment, Karina Barnholt Klepper for aid in using FTIR spectrometer and some final corrections and Kristin Bergum for aid in using XRF equipment.

I would also like to thank the rest of the students and staff in the thin films group in SMN, and also everybody else who took part of more or less scientific discussions in the lunch room. Many good ideas were proposed, and bad ideas rejected, while drinking tea.

Finally I am thankful to my wife, Gunn Marit, for the patience and support she has given me throughout my time at UiO. This would not have been possible without your love and support.

March 2014, Krokstadelva

Joachim Svendsen

Abstract

This work focused on creating luminescent thin films that emit green light on irradiation of UV-light. The thin films were deposited with atomic layer deposition using $Tb(thd)_3$ as a cation precursor. Tb^{3+} ions are used as luminescence activators in the thin films and emit green light.

Two series of films were deposited: One series was based on varying the terbium content in a titania matrix with the $Tb(thd)_3$ + O_3 and $TiCl_4$ + H_2O precursors. The second series was of organic-inorganic hybrid films deposited at different temperatures with $Tb(thd)_3$ + 1,4-bdc as precursors. Characterization of the films consisted of ellipsometry for thickness and optical properties, X-ray diffraction and FTIR for and crystallinity microstructure, X-ray fluorescence for elemental composition, UV-vis spectroscopy for light absorption and investigation of photo luminescence.

Highly luminescent films were obtained when using $Tb(thd)_3$ + 1,4-bdc, while no luminescence was observed for the Tb:TiO_2 films due to oxidation of Tb^{3+} to Tb^{4+}.

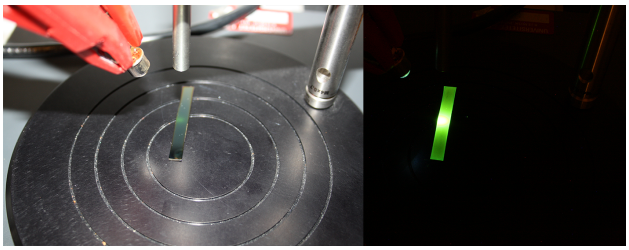

Figure 1: Photo of measurements of luminescent thin film sample.

Abbreviations

1,4-bdc 1,4-benzene dicarboxylic acid. 12, 31–33, 48–53, 58, 63–65, 67, 73–75

ALD Atomic Layer Deposition. 6–8, 10–15, 26, 27, 29, 31–33, 38, 40, 41, 46, 48, 49, 53, 54, 61–63, 66, 73

CVD Chemical Vapor Deposition. 8, 13, 41, 49

FTIR Fourier Transform Infrared Spectroscopy. 35, 54, 56, 64, 65, 67

PL Photoluminescence. 3, 5, 9, 10, 36, 40, 42, 44–47, 58, 59, 63, 64

PV Photovoltaic. 11

QCM Quartz Crystal Microbalance. 7, 8, 26, 27, 38, 49, 50, 52–54, 65, 67, 73, 74

thd 2,2,6,6-tetramethyl-3,5-heptanedion. 7, 8, 12, 16, 31, 33, 38–43, 46–53, 61–63, 66, 67, 73, 74

UiO Univsersitetet i Oslo. 8, 12, 31

UV/VIS Spectroscopy with ultraviolet, visual and near infrared light. 19, 25, 43, 47, 57, 58, 65, 66

XRD X-Ray Diffraction. 21, 22, 34, 39, 40, 65, 66

XRF X-Ray Fluorescence. 24, 25, 34, 42

Contents

1 Introduction

Looking back at the early studies of light-emitting materials show the origins of the terms used for luminescent materials. The study and use of luminescent materials has changed several times. Perhaps the biggest change came with Einsteins proposed light particle, the photon. Light with discrete values of energy described energy processes of elements in support of the new physics of quantum theory.[1] The Bohr atomic model, introduced in 1913, was also an important development that aided in the understanding of the mechanism of luminescence. Luminescence has since been used in various technologies such as displays, lighting and safety equipment and is a well studied phenomenon in modern science.

Energy production from renewable sources, such as solar energy, is emerging as one of the most important areas of study. Photo voltaic (PV) panels for solar energy production are optimized for absorption of photons with an energy close to the band gap of the materials used. The efficiency of the PV panels can be increased by converting the energy of light from the solar spectrum to fit closer with the band gap of the panels. This requires the use of light conversion materials that absorb high energy photons and emit lower energy photons (UV→visible light), called down conversion, or absorb low energy photons and emit higher energy photons (IR→visible light), called up conversion.

Light conversion materials have two advantageous effects on efficiency of PV panels. Photons with much higher energy than the band-gap of PV cells excite the electrons to much higher energy levels than the conduction band. The excess energy is usually transferred to the material causing the temperature of the PV-cell to increase. At high temperatures silicone based PV-panels loose efficiency at around 10% for every 10°C higher temperature. In addition down conversion of light may split one UV-photon into two visible photons, and up conversion may combine two IR-photons into one visible photon, increasing the number of photons usable in energy production.

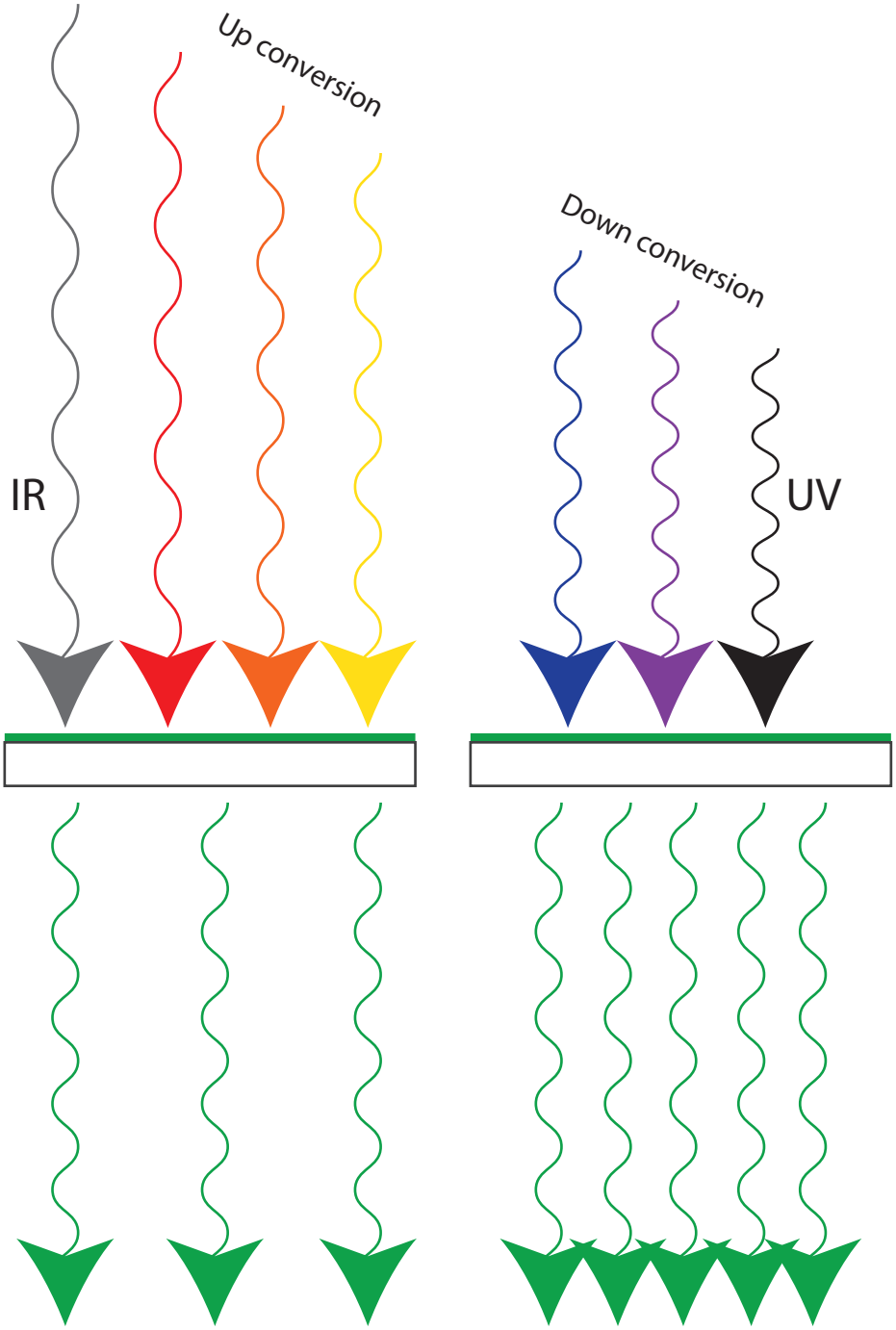

Figure 2: Schematic of how a thin film can enhance the efficiency of photovoltaic panels. Up-conversion of light with insufficient energy to excite electrons to the conduction band, down-conversion of light to make better use of the energy of UV-light.

1.1 Historical perspective

Luminescence is the emittance of light from a substance that is not caused by the substance being hot. There are several types of luminescence and the mechanism of exciting the substance determines the type. Photoluminescence (PL) is the emission of light where the excitation energy comes from the absorption of light. Traditionally PL has been divided into two different mechanisms, phosphorescence and fluorescence.

1.1.1 Phosphorescence

Phosphorus is the Greek word for the planet Venus meaning "light bearer". Since the middle ages it was used for materials that glow in the dark after exposure to light. The element Phosphorus was named because it emits light when exposed to air though it is a bit of a misnomer. Emission of light in the case of elemental phosphorus is due to the slow burning of the element in air, not PL.[2]

The first man-made phosphorescent material was a mineral collected near Bologna that was phosphorescent after calcining. The calcined mineral, named bolognian stone, was prepared by Vincenzo Cascariolo between 1602 and 1604. Cascariolo was a cobbler who dabbled in alchemy and showed his new phosphorescent material to other well known scientists and alchemists. The recipe was first published by Pierre Potier in *Pharmacopoea Spagirica* (1612)[3]

1.1.2 Fluorescence

The first time the term "fluorescence" was used was in a scientific paper by G.G.Stokes called *On the Change of Refrangebility of Light* from 1852.[2] In a series of experiments, some of which were reproduced from other scientists experiments, Stokes observed that UV light caused a solution of sulphate of quinine to emit blue light. In the article he calls the phenomenon *dispersive*

reflexion but in a footnote declares to not like the term. He proposes the term *fluorescence* from flourspar, analogous to the term opalescence derived from the optical effects of opals.[4]

Long before Stokes coined the term fluorescence, scientists were measuring the time gap between when a sample was being irradiated with light to it stopped emitting light. Becquerel considered phosphorescence and fluorescence to be the same phenomenon and advocated that the term fluorescence be abandoned. Despite this the term fluorescence was adopted widely by scientist doing experiments on the nature of light emission.

In 1744 Beccari constructed an instrument that made it possible to measure down to 1/10 of a second. By 1858 Edmond Becquerel had measured a time difference of 10^{-4}s. Though fluorescence is now considered to be light that is emitted within 10^{-8}s of irradiation it can be argued that the difference lies in the mechanism involved in the electronic relaxation that causes the emission of light. Fluorescence could then involve relaxation of electrons without any forbidden relaxations and phosphorescence involves relaxation of electrons where reversal of electronic spin, or other processes where the result is an illegal electron relaxation, delays the relaxation.

1.1.3 Early application

Perhaps the first use of photoluminescence was with identifying counterfeit medication for the kidneys. Wood from a tree later called *Lignum Nephriticum* from Mexico was used by the Aztecs to treat kidney and urinary diseases. The medicine was scarce and expensive and so it was important to have a method to confirm the genuine medicinal wood. A Spanish physician, Nicolás Monardes, wrote about the wood in 1565:

> Make sure that the wood renders water bluish, otherwise it is a falsification. Indeed, they now bring another kind of wood that renders the water yellow, but it is not good, only the kind that renders the water bluish is genuine. (in Spanish in the original)[5]

Figure 3: A piece of *Lignum Nephriticum* dropped into an alkaline solution and illuminated with a UV hand lamp.[6]

1.1.4 Modern physics

Two advances in physics have had substantial impact on the study of PL; the particle nature of light and the Bohr atomic model.

The particle model for light developed in quantum physics determines that the energy of light is quantified. Each quantum of light is called a photon, coined by Einstein, and is a particle with a mass of $m = 0$. The energy of a photon is determined by the wavelength of the light: $E_p = \frac{hc}{\lambda}$ where h is Planck's constant and c is the speed of light. Using the energy of photons, the mechanism of interaction between light and matter can be further determined.

The Bohr atomic model aided scientists greatly in understanding how light interacts with matter. Bohr postulated that electrons orbit the nuclei of atoms in a circular manner and maintain the same orbital without loosing energy, and when an electron jumps from one orbital to an orbital with lower energy a photon is emitted with an energy that matches the energy lost in the atom. When hydrogen gas is irradiated with a spectrum of light, some of the light is absorbed and excites the hydrogen atoms to a higher energy. Atoms that relax to a lower energy level emit photon with energy $E_f = \frac{hc}{\lambda}$ equal to the difference in energy levels. This is the mechanism behind most

types of spectroscopy, which for example is used to determine what elements are contained in a sample.

In addition to the excitation and relaxation process for absorption and emission of light, charge transfers are also involved in light-energy transaction in molecules. Charge transfer absorption moves an electron from one part of a molecule, the donor, to another part of a molecule, the acceptor. This type of absorption and emission typically has less intensity than processes involving the energy levels of electrons in a single atom.

1.2 Prior art

Using Tb^{3+} ions as luminescence emitters is fairly common in for example luminescent lighting and is therefore a fairly well studied phenomenon. Nanoparticles of titanium oxide doped with terbium have been produced and show luminescence properties.[7] Photoluminescent thin films have been deposited with Atomic Layer Deposition (ALD) containing terbium(III) as luminescent centers by Tammenmaa et al.[8;9] In depth studies of thin films of terbium oxide deposited with ALD are not to be found in litterature. Metal hybrid thin films have been the subject of some studies, though not using terbium as the cation. The following will therefore contain results that covers prior art to certain aspects of this work.

1.2.1 Titanium oxide thin films

Titanium oxide films produced with ALD from $TiCl_4$ and water is a well studied system, and thoroughly documented with regards to the surface reactions and its optical and microstructural properties.

Aarik et al.[10] examined the microstructure of films grown from $TiCl_4$ and H_2O at various deposition temperatures (T_d). Below $T_d = 165°C$ the films are amorphous and at lower temperatures they also contain some chlorine, indicating incomplete reactions on the substrate surface. In the region of 165-

350°C the films crystallized with an anatase type structure of titanium oxide. Also, above 165°C the films no longer contain chlorine. Above 350°C the films consisted of both the anatase and rutile phases of TiO_2 with an increasing ratio towards more rutile for higher temperatures. The "high-pressure" TiO_2-II phase can be deposited at substrate temperatures of 375-550°C by carefully controlling the pulse parameters of H_2O.[11]

In situ Quartz Crystal Microbalance (QCM) experiments performed by Aarik et al.[12] indicate a complex set of reactions and processes on the surface. The most relevant result for this work is with a deposition temperature of $T_d = 300$°C and shows that close to four chlorine atoms are adsorbed on the substrate for each titanium. This indicates that $TiCl_4$ may be adsorbed on the substrate, or that volatile $Ti(OH)_xCl_{4-x}$ is formed during the $TiCl_4$ pulse. At T_d below 200°C and above 350°C the amount of chlorine adsorbed onto the surface decreases and growth rate increases. The increase in growth rate is probably due to a higher concentration of hydroxide groups on the surface at lower temperatures and faster decomposition of adsorbed species at higher temperatures.[12]

1.2.2 Terbium oxide thin films

There are very few studies reporting the properties of ALD films of terbium oxide. The only study found that reports any experimental information on the deposition of terbium oxide thin films using Tb(2,2,6,6-tetramethyl-3,5-heptanedion (thd))$_3$ + O_3 as precursors is Hansen et al.[13] It shows a series of experiments depositing lanthanide oxide films using most of the lanthanide elements, including terbium. The lanthanide precursors were $Ln(thd)_3$ and most of the experiments in Hansen et al. excluded the use of terbium oxide thin film. The terbium oxide thin film deposited used $Tb(thd)_3$ and O_3 as precursors with pulse times of 1.5 and 4 seconds respectively, and purges for both precursors of 1.5 seconds. Visual inspection of the film revealed inhomogeneous growth of the film with thickness gradients, and the thickest areas were at the gas inlet end of the reaction chamber. Comparison of

the growth rate with the other lanthanide oxide films showed a much higher growth rate for the terbium oxide film. The crystal structure was determined to be Tb_6O_{11} unlike most of the Ln-oxides which were of a cubic Ln_2O_3 structure.

Terbium oxide thin films have also been deposited using a laser-assisted metal-organic Chemical Vapor Deposition (CVD) technique by Meng et al.[14] Deposition of terbium oxide thin film was carried out at a pressure of 1 Torr at 150°C using $Tb(thd)_3$ as precursor. The precursor was allowed to sublimate onto a substrate and photodissociation was accomplished with the assistance of a laser beam. The resulting films consisted mostly of oxides with minor amounts of carbides. The chemical processes of the deposition and dissociation were studied extensively using laser photo-ionization mass spectrometry. Optical properties of the terbium oxide thin film were not investigated.

1.2.3 Organic-inorganic hybrid thin films

Organic-inorganic hybrid thin films deposited with ALD is still a relatively new field of study. Klepper et al.[15] have studied hybrid metal-organic thin films deposited using ALD with both linear and aromatic organic molecules as anions. The inorganic cations used are aluminum, zinc and titan.[15;16] Others in the research group in the Univsersitetet i Oslo (UiO) have used cobalt and manganese. This work is the first study of organic-inorganic hybrid film containing terbium.

Growth rate of the hybrid films deposited with ALD are in general far higher than for oxide films. In situ QCM experiments show self limiting growth despite the high growth rate. The growth is generally highest at low temperatures and is reduced with increasing temperature. The cause for this reduction in growth rate is hypothesized to be due to thermal motion preventing adsorbed molecules from assembling into dense structures. This is supported by measurements showing that films grown at higher temperatures have lower density than films grown at lower temperatures.

1.2.4 Terbium doped titanium oxide thin film

Wijcieszak[17] and Kaczmarek et al.[18] have investigated and characterized the luminescent properties of thin films of titanium oxide doped with terbium. The films were deposited using a magnetron sputtering process at low pressure oxygen atmosphere from metallic targets. Doping levels for the films characterized were at atomic % of 0, 0.4, 2.0 and 2.6 with a thickness of 377, 423, 533 and 585 nm respectively.

The films were polycrystalline with an average crystallite size of 8.7 nm and the crystal structure somewhat dependant on doping levels and characterization method. XRD 2θ analysis showed that the 0.4 at. % film had anatase structure while the rest of the films hat rutile structure. Analysis using Raman spectroscopy revealed that all films had a mixture of amorph, anatase and rutile structure.

Transmission of visible light of the Tb-doped titania films was about the same as the non-doped film at 80%. The absorption edge of the 0.4 at. % film was at a shorter wavelength as expected due to the dominance of anatase structure of the film, while the 2.6 at. % films absorption edge was shifted slightly towards longer wavelengths.

The only sample of the study that displayed PL was the 2.6 at. % film. This appears to be the first case of photoluminescence emitted from Tb^{3+} ions in a titanium oxide rutile matrix. The challenges of terbium luminescence in rutile stems from defect states with lower energy levels that are needed to excite the terbium ions. Energy transfer from titanium oxide to terbium luminescent centers must originate in the conduction band or the PL is excluded. The authors concluded that the positioning of Tb^{3+} ions on the surface of the rutile nanocrystallites allowed direct transfer of energy to the luminescent centers.

Figure 4 shows the energy processes involved in excitation and emission of photons from the Tb-doped titanium oxide film. The most intense PL has a wavelength $\lambda = 545$ nm which corresponds to relaxation from $^5D_4$ to $^7F_5$ of

the terbium ion.

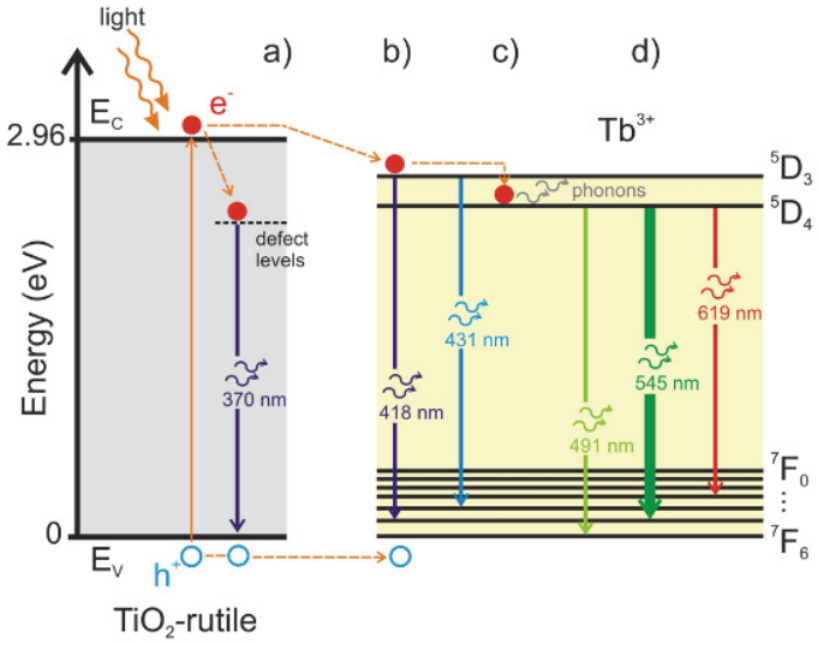

Figure 4: Energy diagram showing the mechanisms of a) radiative recombination of matrix defect levels, b) radiative transition from $^5D_3$ to $^7F_5$ and $^7F_4$ levels, c) non-radiative transition between $^5D_3$ and $^5D_4$ levels and d) radiative transition from $^5D_3$ to $^7F_6$, $^7F_5$ and $^7F_3$ levels.[17]

1.3 Current work

The main focus of this work is to synthesize luminescent thin film using the ALD method and investigating the structural and optical properties. The ultimate goal is to produce thin films of a host matrix doped with lanthanide ions that show PL with red, green and blue light.

The potential energy of electrons excited by photons in a photo electric device is determined by the band gap of the materials. When photons with a higher energy than the band gap are absorbed, the surplus energy heats up the solar panels and is lost with regard to electric energy production. Photons with a lower energy than the band gap do not contribute to electric energy at all, only heat. It is therefore difficult to achieve high efficiency energy production

from solar panels. An ideal light conversion material for Photovoltaic (PV) electric production would absorb a UV photon and emit two or more photons ideally suitable for energy production. Also it would absorb two or more IR photons and emit a single photon ideally suitable for energy production. The process of splitting a photon into several photons of lower energy is called *down conversion* and combining photons into a single photon with higher energy is called *up conversion*.

Down shifting of light usually involves a sensitizing material that enhances the absorption of light, and a transfer of energy to luminescence centers. The luminescent centers, in this work Tb^{3+} ions, absorb energy from the surrounding matrix and emit light with wavelengths characteristic for the ions used.

The initial plan involved using TiO_2 as a host matrix for lanthanide ions. The purpose of utilizing a host matrix is to take advantage of its large band-gap to increase absorption of high energy photons. Titania has several morphologies with slightly different band-gaps allowing making refinements to the properties of the thin films. Different materials may also be suitable has host matrices and used for comparison with titania.

Lanthanide ions are commonly used as emission centers for luminescent materials. The luminescent properties of the lanthanide ions are largely dependant on their oxidation states. Light emissions for commonly used lanthanides are red for Eu^{3+}, blue for Eu^{2+}, green for Tb^{3+} and blue/yellow for Ce^{3+}. The emissions usually originate from the shielded f-shell electrons allowing the centers to maintain their luminescent properties in hosts with different chemical properties.

The use of ozone during deposition may be an issue for the oxidation states of the lanthanide ions. Maintaining the oxidation state of the luminescent centers will therefore be important part of the work, either by controlling the oxidation state in situ during deposition or reduction of the as deposited films.

The challenges encountered due to use of ozone in the ALD process caused

focus to change. Instead of developing thin films that emit different color the goal was to produce luminescent thin films with terbium(III) ions. A decision was made to seek out alternate processes that eliminate ozone from the ALD deposition. In the process of researching alternatives an organic-inorganic metal hybrid process using $Tb(thd)_3$ + 1,4-benzene dicarboxylic acid (1,4-bdc) as precursors was attempted. Other work in the chemistry department at UiO had successfully deposited thin films with ALD using metal-thd complexes with organic precursors.

2 Methodology

2.1 ALD

ALD is a type of CVD and was initially called atomic layer epitaxy (ALE) or atomic layer CVD. "Epitaxy" has previously been used to describe growth that repeats the crystal structure, and the literal translation from Greek is "on arrangement"[19]. Films deposited with this method are usually polycrystalline or amorphous and atomic layer deposition is considered a more suitable name[20].

2.1.1 Brief History

The ALD technology was developed in the 1970s in Finland by Tuomo Suntola with the first patent application filed in Finland in 1974. The motivation for developing the technology was to provide thin pin-hole free films for the production of electroluminescent flat panel displays. Interest in the technology has increased from before 1990, when fewer than 100 articles were published per year, to about 900 per year in 2010.[20]

2.1.2 Basic Principles

The difference between the CVD and ALD methods is that CVD combines the precursors in the gas-phase in the reaction chamber and the reaction is strongly affected by the temperature of the substrate. For CVD growth the desired reaction must be close to equilibrium. A slight difference in temperature, or in the kintetics of the molecules on the substrate, causes enough change in the equilibrium of the reaction for the precursors to react. The process is very sensitive to changes in temperature and pressure which may cause the precursor to react before being absorbed onto the substrate, often producing a fine powder. A clear disadvantage with CVD is that the films often have a thickness gradient due to the flow pattern of the precursor

gases over the substrate.

ALD utilizes separation of the volatile precursors in order to guide the growth to the substrate. The gas-phase precursors fill the reaction chamber one at a time and react with the surfaces in the reaction chamber. Between the precursor pulses, an inert gas is used to flush excess precursor out of the reaction chamber. The films are grown by repeating the self-limiting half reactions between the precursors and the substrate. See schematic of one ALD cycle consisting of $Al(CH_3)_3$ reacting with H_2O producing Al_2O_3 and CH_4 in figure 5.

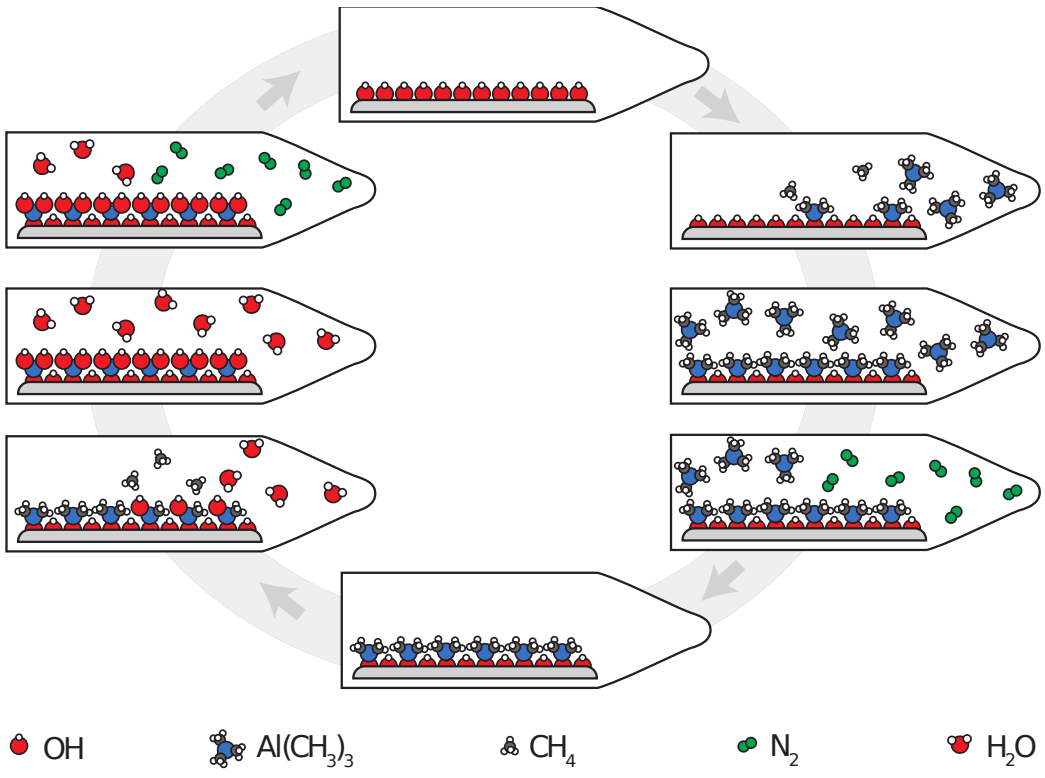

Figure 5: Schematic of one cycle of film growth with ALD. The precursors are $Al(CH_3)_3$ and water, the product is Al_2O_3 and the waste is methane. Nitrogen gas is used to push the precursors through the system.[21]

2.1.3 Precursors for ALD

There are two basic principles governing the properties of precursors used in ALD, vapor pressure and reactivity. ALD precursors, liquid or solid, have to be brought to the gas phase in order to be transported to the reaction chamber and react with the substrate. Solid precursors usually need to be heated to reach sufficient vapor pressure. By using liquid precursors the vapor pressure is not affected by change in surface area, which is the case for solid precursors, allowing for better control over how much precursor is pulsed into the reactor.

A rapid reaction between the precursor and the surface is an advantage in ALD growth due to the self limiting nature of the reactions: rapid reactions allow short cycle times and increased deposition rates. Some precursors used in ALD are therefore quite volatile and react violently in air, which can become a safety concern.

2.1.4 Growth Mechanism

The limiting factor in film growth by ALD is the coverage of the precursors onto the substrate. Most systems have a growth rate of less than one monolayer of film per cycle.

Large and heavy ions sometimes require large organic ligands for the molecules to be brought into the gas phase. The ligands increase the precursors volatility at higher temperatures allowing sublimation without decomposition occurring. Precursor molecules adsorbed onto the substrate can take up considerable space due to the size of the ligands, illustrated in figure 6. Looking at how much shadow the molecule would cast on the substrate can be used as a model for how much precursor it takes to cover the substrate, which is then used to approximate the growth rate.

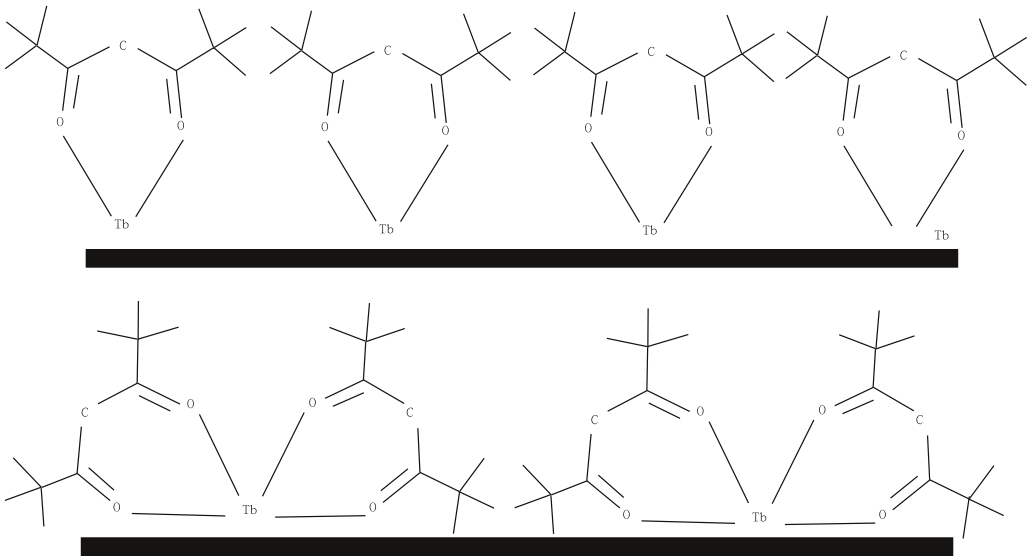

Figure 6: 2D schematic model of how precursors with large organic ligands, such as $Tb(thd)_3$ are adsorbed on the substrate surface. Top shows an example where two ligands react on the surface and one remains. Bottom shows an example where one ligand reacts on the surface and two remain.

2.2 Ellipsometry

Ellipsometry is the term used for the analysis of the elliptical polarization of a reflected beam of light. There are several variations of ellipsometry, where the light used is monochromatic, where the wavelength is in the UV, visible or near IR region or where a spectrum of wavelengths is used. The method can be used to analyze a wide range of thin film types and materials and is a rapid and accurate method of investigating thickness of films. It can also be used for real-time monitoring of the growth processes, investigation of structures that vary continuously during growth and determination of alloy composition and growth rate of each layer. Description of spectroscopic ellipsometry is adapted from selected chapters of Fujiwara's book on the subject. [22]

Ellipsometry measurements are done by measuring the change in polarization parameters of polarized light reflected off a sample. Reflection of light on a sample depends on the refractive indices of the materials that make up

the reflective interface and of the polarization of the incident light. Polarized light reflected on or transmitted in a sample is classified as s-polarized or p-polarized light. With p-polarized light the electric field of incident and reflected light oscillate in the same plane, called the plane of incidence. For s-polarized light the oscillations are perpendicular to the plane of incidence.

When light is reflected off a surface at an angle s-polarized and p-polarized light are reflected differently. The difference is due to the orientation of the dielectric oscillations of the material. If the angle of the oscillations is the same as the angle of incident and reflected light the reflectance of p-polarized light is reduced or completely disappears. When the reflectance of p-polarized light is zero at a certain angle it is called the Brewster angle θ_B.

As seen in figure 7 $\theta_B + \theta_t = 90°$ at $\theta_B = \theta_i$ so that $\theta_t = 90° - \theta_B$. Using Snells law ($n_i \sin\theta_i = n_t \sin\theta_t$) and trigonometry to determine that $\sin(90° - \theta) = \cos\theta$, and combine it with Snells law $n_i \sin\theta_B = n_t \cos\theta_B$. This can be rewritten to form what is called Brewster's law:

$$\tan\theta_B = \frac{n_t}{n_i} \tag{1}$$

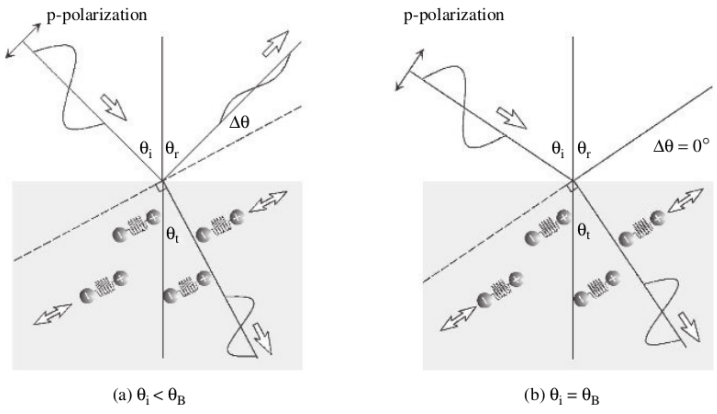

Figure 7: Electric dipole radiation of incident and reflected light at (a) $\theta_i < \theta_B$ and (b) $\theta_i = \theta_B$[22]

If the reflectance of p-polarized light is not zero but reaches a minimum it is called the pseudo Brewster angle $\theta_{B'}$. The Brewster angle is often called the polarization angle because of its polarizing effects on the reflected light. Due to the larger differences in reflectance of s- and p-polarized light at θ_B and $\theta_{B'}$ ellipsometry measurements is performed at angles at or near the Brewster angle.

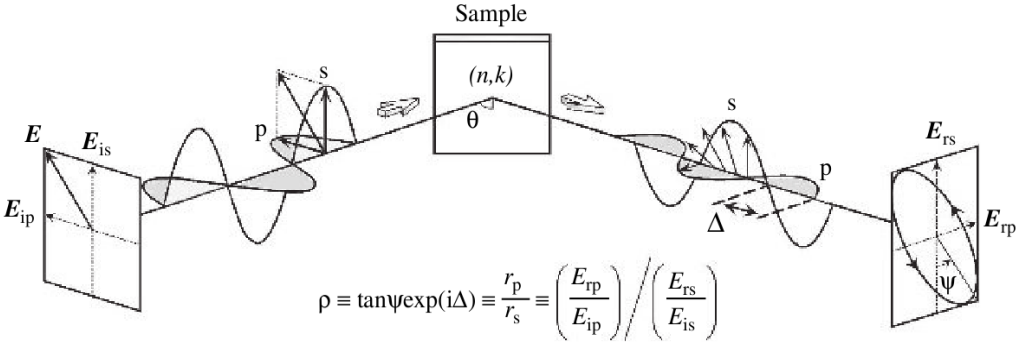

Figure 8: Measurements in ellipsometry are use linearly polarized light that is reflected off the measure sample. The reflected light beam has a different amplitude ratio Ψ and different phase of s- and p-polarized light Δ.[22]

The actual measurement of ellipsometry is ρ, which includes (Ψ, Δ) where Ψ is ratio of reflected s- and p-polarized light and Δ is the phase difference of reflected s- and p-polarized light. Schematic of the polarization and phase changes in figure 8. The relation between the measured value, (Ψ, Δ) and the ratio of reflected polarized light is given by:

$$\rho \equiv \tan\Psi \exp(i\Delta) \equiv \frac{r_p}{r_s} \tag{2}$$

2.2.1 Calculations

A optical model such as the Cauchy function (3) is fitted to the calculated (Ψ, Δ) by varying the variables (A, B, C). When optical constants have been extracted from the optical model the thickness can be calculated using

Bragg's law.

$$n = A + \frac{B}{\lambda^2} + \frac{C}{\lambda^4} + \dots \tag{3}$$

Because the optical constants are modeled rather than actually measured a proper measurement of the optical constants to back up the ellipsometry data is advised. The optical constants extracted from the models may be erroneous and should be checked to verify that they adhere to the physics involved. The refractive index used in the model must increase when the wavelength of light involved decreases.

2.3 Spectroscopy with ultraviolet, visual and near infrared light (UV/VIS)

With UV/VIS the absorption of light can be used to observe the available electronic transitions of the material. Some typical electronic transitions are organic $\pi \rightarrow \pi^*$, charge transfer on ionic complexes, d-electron transition for transition metals and f-electron transition for lantanides and actinides. This section is based on Workman and Springsteen's *Applied Spectroscopy: A Compact Reference for Practitioners* and Gauglitz and Vo-Dinh's *Handbook of Spectroscopy*.[23;24]

In UV/VIS the light source usually emits a broad spectrum. Depending on the working range of the spectrometer there are usually several broad band light sources that each work in a different range. The broad band of light must be dispersed with a monochromator that allows mechanically choosing a single wavelength or a small band of wavelengths. The monochromator may use a prism or grating to disperse the band of light into a spectrum. A slit, usually with variable width, is used to select the bandwidth to irradiate the sample with.

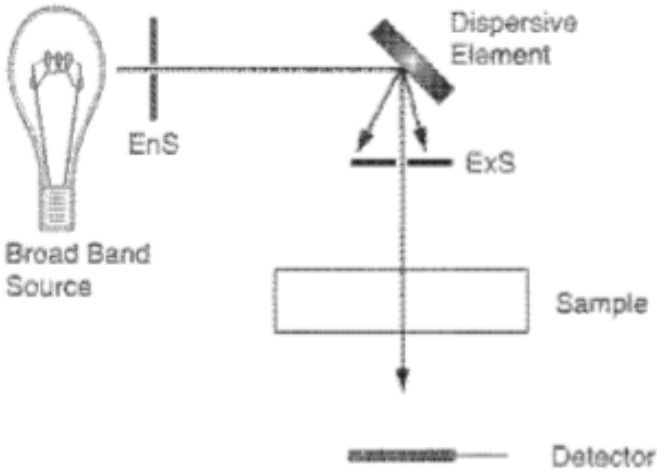

Figure 9: Simple schematic of optical spectrometer showing light source, entrance and exit slits, dispersive element, detector and sample of a single monochromator system.[23]

When the purpose is to measure transmittance where the transmitted light follows the same vector as the incident light, a normal detector is used. An integrating sphere must be used to collect light that was scattered on transmission or by reflection. The inside of an integrating sphere is coated with a powder that scatters all the light inside the sphere. Eventually, all the light will reach the sensor located in one part of the sphere wall.

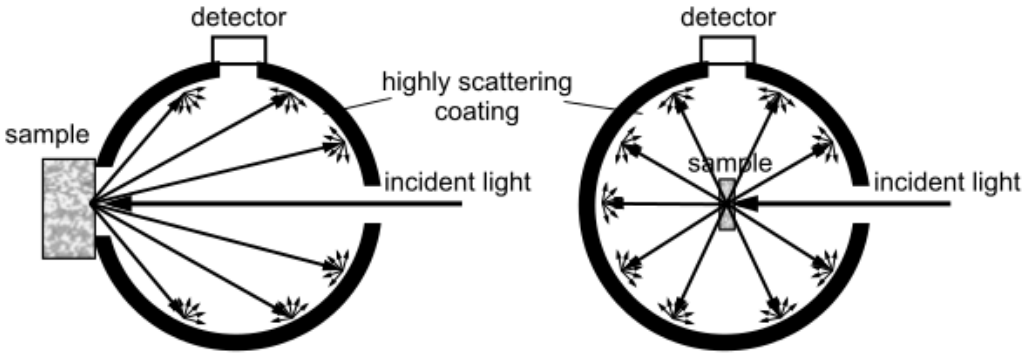

Figure 10: Two types of integrating spheres (also called Ulbricht spheres). One with the sample position on a port to the sphere, one with the sample positioned inside the sphere.[24]

Some instruments use dual beams to measure the relative reflectance or transmittance of the sample where one beam is used as a reference. Single beam instruments need a baseline measurement to find the relative reflectance and transmittance of the sample. The reflectance baseline measurement uses a material with 100% reflectance such as $BaSO_4$ while the transmittance baseline just allows the light into the integrating sphere.

Any light that was not reflected by the sample or transmitted through the sample must have been absorbed in the sample. Thus it is simple arithmetic to calculate how much light the sample absorbed.

$$I_a = 1 - I_r - I_t \tag{4}$$

In equation 4 I_a is absorbed light, I_r is reflected light and I_t is light transmitted through the sample. Using an integrating sphere allows measurement of diffuse transmission and reflection, which makes the calculation of absorption more accurate.

2.4 X-Ray Diffraction (XRD)

XRD has been used in characterization of materials since Laue created the first diffraction pattern of a crystal. The method has been used for many important discoveries, such as the double helix structure of DNA, and has gone through many improvements since. This section is based on *Elements of Modern X-ray Physics* by Als-Nielsen et.al.[25]

Shortly after the discovery of X-rays by Röntgen in 1895 it became apparent that the rays were easily transmitted through some materials, such as paper and wood, but not others, such as metals and human bones. It turns out that X-ray absorption depends on the elements present and varies approximately with Z^4, Z being the atomic number of atoms. This explains the observed variations in interaction phenomena of X-rays with different materials. With the further discovery of a diffraction pattern from a periodic lattice of atoms by von Laue and the early work on crystallography by W.H. Bragg and

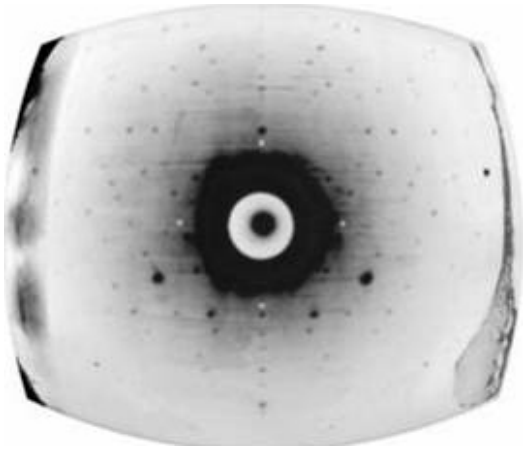

Figure 11: One of the first X-ray diffraction images made by von Laue et.al. using a crystal of ZnS in front of an X-ray beam.[26]

W.L.Bragg in 1912-13 the stage was set for structural characterization of materials using XRD.

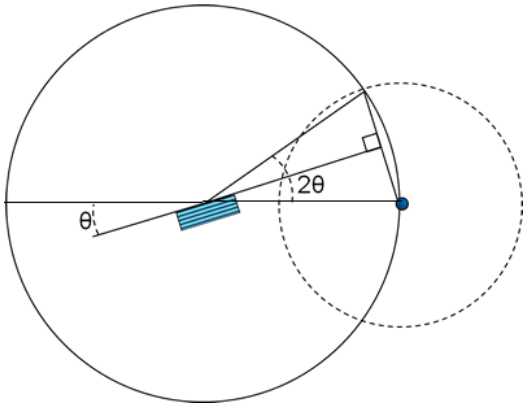

Figure 12: Simple schematic of θ-2θ measurements.[27]

In order to determine the crystal structure of thin films a θ-2θ measurement, also used in powder diffraction, is used. The θ-2θ scan is done with the incident radiation and detection of reflected radiation at the same angle as seen in figure 12. θ refers to the angle of the incident radiation to the sample and 2θ to the angle of the diffracted radiation to the incident radiation. During the scan, the 2θ angle changes through a preset range by moving the detector in a circular path around the sample. Simultaneously the sample

rotates to keep the angle of incident and reflected radiation the same at θ.

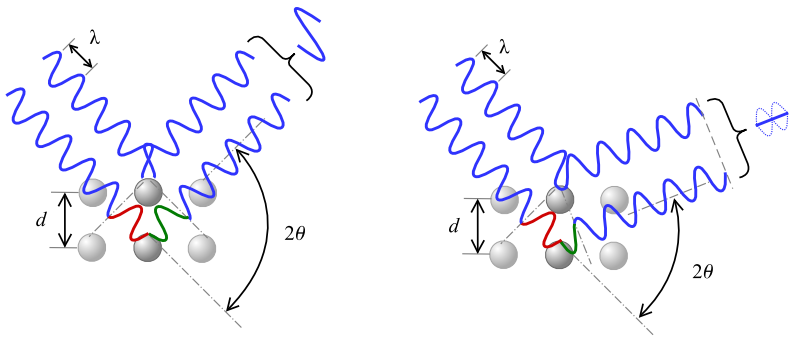

Figure 13: Schematic of Bragg scattering off the atoms in a crystal.[28]

X-rays interact with atoms in a material by reflecting off the atoms in crystal planes in the material. In θ-2θ measurements, the reflections are from planes oriented parallel to the surface and all planes with the same orientation will reflect the radiation. Reflections from all the planes in the crystallites will create an interference pattern due to the differences in distance caused by spacing of the crystal planes. Interference patterns can be modeled using Bragg's law: $d \sin\theta = n\lambda$ where d is the distance between the planes in the crystal, θ is the angle of incident, n is an integer and λ is the wavelength of the radiation. It is obvious from Bragg's law that the lattice parameter of a crystal, here represented by distances between planes, is inversely proportional to the angle θ. It is therefore usual to calculate refinements in unit cell parameters using reciprocal space.

The resulting diffractogram from θ-2θ measurements is often used to simply determine what phase of a material is synthesized. This is usually done by looking for identical patterns in a crystallographic database to find what crystal structure consisting of a particular set of elements causes the diffraction pattern. Several databases contain collections of diffractograms that can be matched to measured diffractograms, two used in this work are EVA plus and Pearson's Crystal Data.

2.5 X-Ray Fluorescence (XRF)

The discovery of X-rays and the subsequent work to determine their nature resulted in the discovery that X-ray sources emit radiation with different energy spectra. This led to the development of XRF which is a simple method of identifying elements and determining the abundance of elements in a sample. This section is base on *Handbook of Practical X-Ray Fluorescence Analysis* by Beckhoff et.al.[29]

The gaps in atomic absorption of X-rays and spectroscopic series of X-rays were discovered by Barkla 1909-1911.[30;31] As sources of X-rays were developed that provided radiation of increased intensity, the accuracy of spectroscopic series also increased. With the development of Bohr's atomic model[32], as yet undiscovered elements were predicted to exist. Hafnium and rhenium are examples of elements isolated as a result of experiments devised because of X-ray fluorescence spectroscopy. Further developments in X-ray sources and detectors resulted in the first commercial X-ray fluorescence spectrometer in 1948.

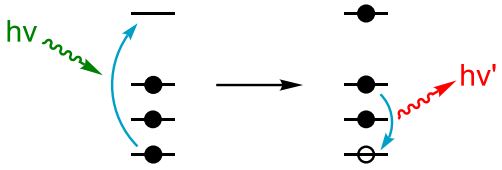

Figure 14: Simple figure demonstrating excitation and emission mechanism used in XRF characterization. Illustration from wikimedia commons.

The basic principle of XRF lies in identifying the characteristic emission spectrum of elements by ionizing the elements with X-rays. An electron from a higher energy orbital recombines with the hole left from the ejected electron and a photon is emitted, a process traditionally called fluorescence. The photons emitted form an emission spectrum that is unique and characteristic for each element allowing identification of elements in a sample.

In order to determine the elemental composition of a sample a relative ele-

mental analysis is needed. There are several analysis methods in use, though the only one really suited for thin films is called "fundamental parameters". It basically involves fitting several sets of equations that model the interactions between photons and atoms. The equations need to be calibrated with standard samples before running an experiment in order to get acceptable results. UniQuant, a manufacturer of XRF analysis software, has refined the calibration of the instrument from the fitting of a curve to the fitting of a straight line. The refinement allows elemental analysis of a mono-layer samples even though the sample and substrate contain common elements. [33]

2.6 Photoluminescence measurements

Photoluminescence is the excitation of a materials energy state via light with the subsequent emission of light from the relaxation of the excited energy. Luminescent materials may be down converting light where the excitation is achieved with higher energy light than the luminescence, or up converting light where the excitation is achieved with lower energy light than the luminescence.

Luminescent materials absorb light in the lattice or in functional groups of the host material, called sensitizers. The absorption may be a property of the host material or may be an enhancement from doped impurities in the material. The sensitizers often have characteristic energies where absorption is the strongest, and which can be found as absorption peaks in UV/VIS. The energy from the excitation is transferred to activators in the material, or the electronic state of the material goes through a non-radiative relaxation, to where the excited state is relaxed and the difference in energy is emitted as light.

The color of luminescence depends on the nature of the activators of the material. Activators consisting of transition metals or compounds are often affected by the electronic structure in the host material and may have different color luminescence in different materials. This allows tuning the materials luminescence color by changing the host material. In some cases

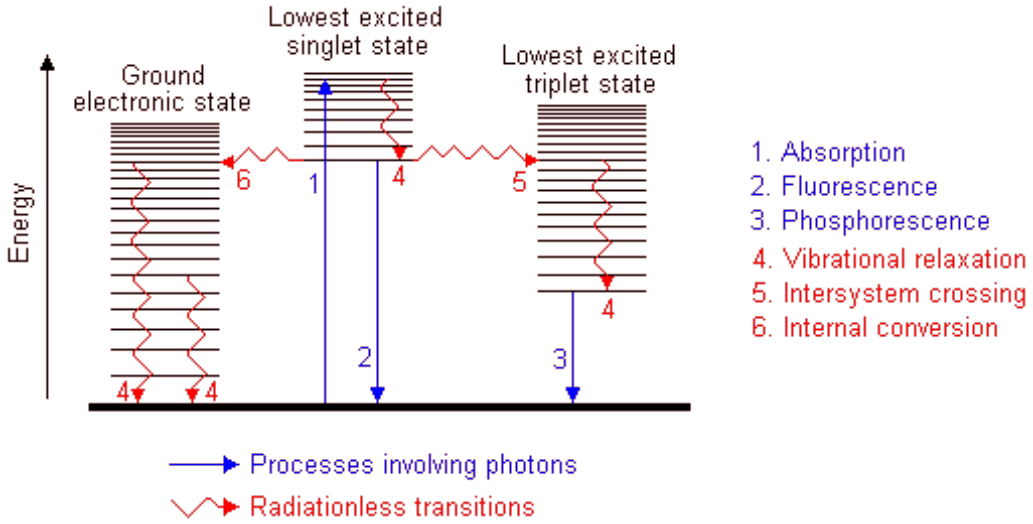

Figure 15: Schematic displaying absorption of photons, non-radiative energy transitions and luminescence in photo luminescence processes.[34]

the activators have characteristic luminescence in which the color of luminescence is unaffected by its surroundings. This is often the case with lanthanide ions where the f-electrons that are the source of luminescence are shielded form their surroundings by higher energy electrons. When working with luminescent materials, the color spectrum and nature of luminescence aids in determination of the luminescent activator in the material.

2.7 QCM

QCM is a method often used for in situ analysis of an ALD process. The resonance frequency of a piezoelectric crystal changes when precursors deposit on the surface of the crystal. Large temperature and pressure fluctuation also have an effect on the frequency and limit the usefulness of QCM for some precursors, such as ozone. The relationship between change in frequency and change in mass is linear and can be calculated with the Sauerbrey equation, equation 5.[35]

$$\Delta f = -\frac{2f_0^2}{A\sqrt{\rho_q \mu_q}}\Delta m \tag{5}$$

Where f_0 is the resonant frequency, A is active area of crystal, ρ_q is density of crystal and μ_q is the shear modulus for the cut crystal used in the QCM experiment.

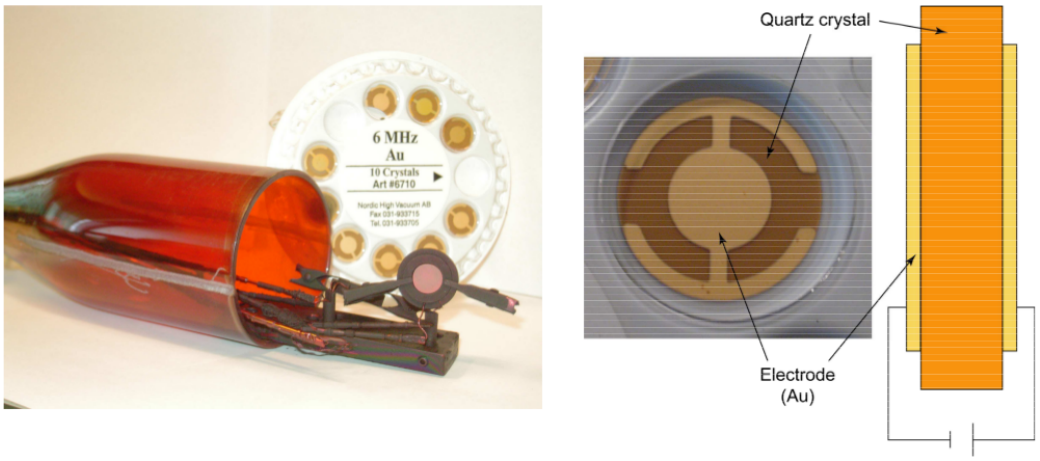

Figure 16: Equipment setup for in situ QCM investigation of ALD processes.[36]

In situ QCM experiments are useful for optimizing pulse- and purge times and determining the half reactions on the substrate. If the density of the as deposited films is known absolute mass increase per cycle per cm^2 can be calculated using data from frequency change during QCM experiment.

2.8 Current-voltage characteristics

Measuring current-voltage characteristics for thin films are performed using different methods depending on the resistivity of the film. Measurement is usually done by setting a maximum voltage and cycling it from 0V to maximum to negative maximum and back up to 0V. For this work the measurement requires a conductive substrate with one electrode on the film and one underneath the substrate.

Films with high density and smooth surfaces use a mercury electrode applied to the film aided by vacuum. With low density or rough surfaces the vacuum

can not apply the mercury electrode, and a small sample of fluid germanium is added to the surface of the film instead. Underneath the substrate a piece of copper tape is sufficient for an electrode.

3 Experimental

3.1 The ALD reactor

The thin films were deposited using a commercial F-120 Sat reactor from ASM Microchemistry Ltd. It is a hot wall type reactor which means the temperature is the same in the entire reaction chamber.

The reactor is constructed out of a large single silica tube capped with a hatch used to insert substrates at one end and the block assembly at the other end. Nitrogen flows into the reactor at either end, 200ml/minute through the valves and 300ml/minute into the outer chamber of the reactor. The valves control the flow of precursor to the reaction chamber and a flow of nitrogen pushes precursor vapor into and through the reaction chamber while pulsing.

Figure 17: Schematic of the interior of a F-120 Sat ALD reactor. Gas flow arrows indicate gas flow during pulsing of precursors. [15]

During purging the flow of gas goes away from the reaction chamber aided by the vacuum pump. The flow of nitrogen into the main chamber of the reactor keeps precursors contained in the triplet through continual flow of nitrogen from the outer chamber into the reaction chamber and triplet.

Figure 18: Schematic of the interior of a F-120 Sat ALD reactor. Gas flow arrows indicate gas flow during purging of precursors. Image adapted from Klepper. [15]

The reactor can make use of solid, liquid and gas phase precursors. Liquid and gas precursors do not usually require preheating and are placed outside the reactor. Solid precursors usually require heating to increase the vapor pressure of the solid, and are therefore placed inside the reactor. If liquid precursors have low vapor pressure at ALD deposition pressures the flow of precursor vapor can be increased using the flow of an inert carrier gas into the flask containing the precursor.

Internally the reaction chamber is divided into 8 zone with heat shields as seen in figure 19. The temperature in each zone is individually controlled and heated with separate elements. Zones 1-4 contain internally placed precursors, zone 5 is a buffer zone between zones 1-4 and zone 6-8. The reaction chamber is located in zone 7 and zones 6-8 are all at the desired deposition temperature T_d.

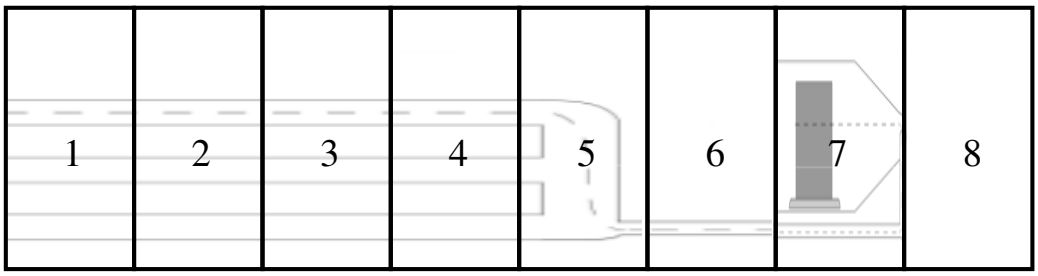

Figure 19: Schematic of the zones in a F-120 Sat reactor. Image adapted from Klepper.[15]

Figure 20 shows the orientation of the substrates in the reaction chamber. Tree substrates were used for each deposition and place at different positions in the reaction chamber. The "front" substrate is placed closest to where the precursors flow into the chamber. The "main" substrate is placed in the "sweet spot" of the reaction chamber, where the depositions conditions are considered to be optimal. The "back" substrate is place in the rear of the reaction chamber where flow of nitrogen gas aids in keeping precursor gases within reaction chamber and exhaust tube.

Figure 20: Reaction chamber used in ALD. Gas flow enters the chamber in the to glass tubes pointing down on the left side and exit to the exhaust to the right. Front substrate on the left, back substrate on the right and main substrate in the middle.

Abbreviation	*Supplier*	*Purity*
1,4-bdc	Fluka Chemical	>99%
$Tb(thd)_3$	Strem Chemicals	>99.9%
$TiCl_4$	Sigma Aldrich	<99.9%
H_2O	UiO	Type II ion exchanged
O_3	UiO	>99.9%

Table 1: Precursors used for deposition of thin films.

3.2 Precursors

Table 1 shows a list of the ALD precursors used in this work.

3.2.1 $Tb(thd)_3$

$Tb(thd)_3$, also called Tris(2,2,6,6-tetramethyl-3,5-heptanedionato)terbium(III), has molecular formula $Tb(C_{11}H_{19}O_2)_3$ and molar mass of 708.74 g/mol. It is an off-white powder than is photo luminescent under UV light. The melting point is 155-156°C and boiling point is 275°C.[37]

3.2.2 H_2O

H_2O used in the deposition is grade II ion exchanged water from the chemical departments Millipore Elix 10.

3.2.3 1,4-bdc

1,4-bdc, also called terephthalic acid, is a white powder with chemical formula of $C_8H_6O_4$ and molar mass is 166.13 g/mol. In air 1,4-bdc sublimates before it melts and the sublimation point is generally reported as higher than 300°C.[38]

3.2.4 $TiCl_4$

Titanium(IV)chloride, molecular formula $TiCl_4$, is a pale yellow liquid with boiling point of 136^{o}C. It is highly reactive to water and water vapor and special care needs to be taken when handling. Products from reaction with water in normal atmosphere are a fine TiO_2 powder and hydrochloric acid.

Refilling the flask containing $TiCl_4$ must be done with proper care under a fume hood. After refilling the flask it is attached to the ALD reactor, which is at low pressure, and any gases in the flask are removed using the vacuum action of the reactor. Hydrochloric acid from reactions with vapor are removed due to vapor pressure being higher.[39]

3.2.5 O_3

Ozone used in the ALD-lab in the chemistry department us produced from oxygen using OT-020 from Ozone Technology. In addition to being used as an anion in ALD reactions it is sometimes used to clean substrates of any remaining organic substances.

3.3 TiO_2:Tb thin films

The TiO_2:Tb films where produced by alternating between the deposition of TiO_2 films and the $Tb0_2$ films.

TiO_2 films deposited with ALD is a thoroughly studied process where the reaction mechanisms, growth rate, phase transitions and optical properties are well known.(2do cite) The precursors for the process are $TiCl_4$ and water, and the waste product is HCl. Both precursors are placed at room temperature outside the reactor and have sufficient vapor pressure to provide precursor gas to the reactor.

Titania films have known growth rates and sensitivity to leaks in the. Deposition of titanium oxide films was therefore used throughout the experimental work to check that the reactor was in satisfactory working order.

The TbO_2 films terbium precursor is $Tb(thd)_3$ ($Tb(thd)_3$), a white powder placed inside the reactor at Ozone from a was used to react with the organic ligands of the terbium precursor effectively burning them away.

The initial test series of TiO_2:Tb was deposited with a set number of cycles for every sample. The mixture of TiO_2 and TbO_2 layers was achieved by alternating deposition of terbium and titanium oxide layers. The layer ratios were 19:1, 9:1, 7:3, 1:1, 3:7 and 1:9 and the deposition of layers was arranged to get the different layers as even as possible.

3.4 $Tb(bdc)_3$ thin films

The metal-carboxylic acid ALD system is fairly well studied system, though this seems to be the first published work using terbium(III) as the cation and 1,4-bdc as anion. The deposition of Tb(1,4-bdc)$_3$ series focused on varying the deposition temperature.

3.5 Tb(III) salts

Various terbium(III) salts were synthesized to investigate differences in luminescence of Tb^{3+} in differing environments. Terbium(III,IV) oxide (>99.9%) from Unocal Molycorp, was refluxed in acid over night, one batch in hydrochloric acid, one in sulphuric acid. The resulting solutions were dried to precipitate white powder consisting of $TbCl_3 \cdot 6\,H_2O$ and $Tb_2(SO_4)_3 \cdot 8\,H_2O$.

$Tb(NO_3)_3$ from Aldrich (>99.9%) was dissolved in water and mixed with a saturated solution of potassium fluoride. The resulting gel was diluted until the solution was clear with a white powder at the bottom of the glass. The powder TbF_3 salt, was filtered and dried.

3.6 XRD

Microstructural characterization was performed using a Siemens D5000 X-ray diffractometer using CuK1 radiation as filtered by a Ge(111) monochromator. Sample holders with sticky putty were used to hold the Si substrates containing films.

The diffractograms were analyzed with EVA from Bruker-AXS to find the structure of the films. In some cases EVA was unable to find suitable structures for the films. Therefore some scans were analyzed by comparing peak patterns of different structures using *Pearson's Crystal Data Crystal Structure Database for Inorganic Compounds* from Crystal Impact GbR.

3.7 XRF

The chemical stoichiometry was measured by X-ray fluorescence on a Phillips PW2400 Spectrometer and interpreted with the Uniquant analysis software in the Department of Geosciences, UiO.

3.8 Fourier Transform Infrared Spectroscopy (FTIR)

The FTIR spectrometer is a Bruker IFS 66 VS spectrometer. Prior to scanning a sample a baseline scan was done on a substrate from the same Si wafer as the substrate on which the thin film was deposited. Baseline and sample scans were carried out with care to keep the conditions as similar as possible, as running the vacuum pump for differing lengths of time may result in differing water vapor content in the spectrometer.

3.9 Ellipsometry

Thickness of the thin films was found via ellipsometry using an alpha-SE spectroscopic ellipsometer to measure the optics of the film and Complete Ease from to calculate a model to match the measurements, both from J.A. WOOLLAM CO. INC. The Cauchy function was used to fit the optical model.

Figure 21: The J.A. WOOLLAM CO. INC. ellipsometer.

3.10 Light Absorption of films

Investigation of absorption of light of deposited films was done using a Shimadzu UV-3600 photospectrometer with an integrating sphere. The absorbency of the films was then calculated by subtracting the relative intensity of reflected and transmitted light.

3.11 Luminescence of films

Initial investigation of PL was performed using a CAMAG hand-held UV-lamp with two settings, $\lambda = 254$ nm and $\lambda = 366$ nm, to excite the samples in a darkened room. Presence, or absence, ofPL was then determined visually.

Photoluminescence of thin films and compounds was measured using a USB4000 Miniature Fiber Optic Spectrometer and recorded with SpectraSuite, both from Ocean Optics Inc. The samples were excited using LED from PHOTON systems which emitted UV-light at $\lambda = 280$ nm. The LED was powered by a Powerbox power supply from Delta Electronica. The setup is not suited to calculate quantum yield, but it is possible to measure the intensity of samples relative to each other by carefully controlling the position of the equipment.

Some samples were investigated using a 325 nm CdHe laser for excitation and an Ocean Optics USB4000 photospectrometer in the 350-1000 nm range for detection.

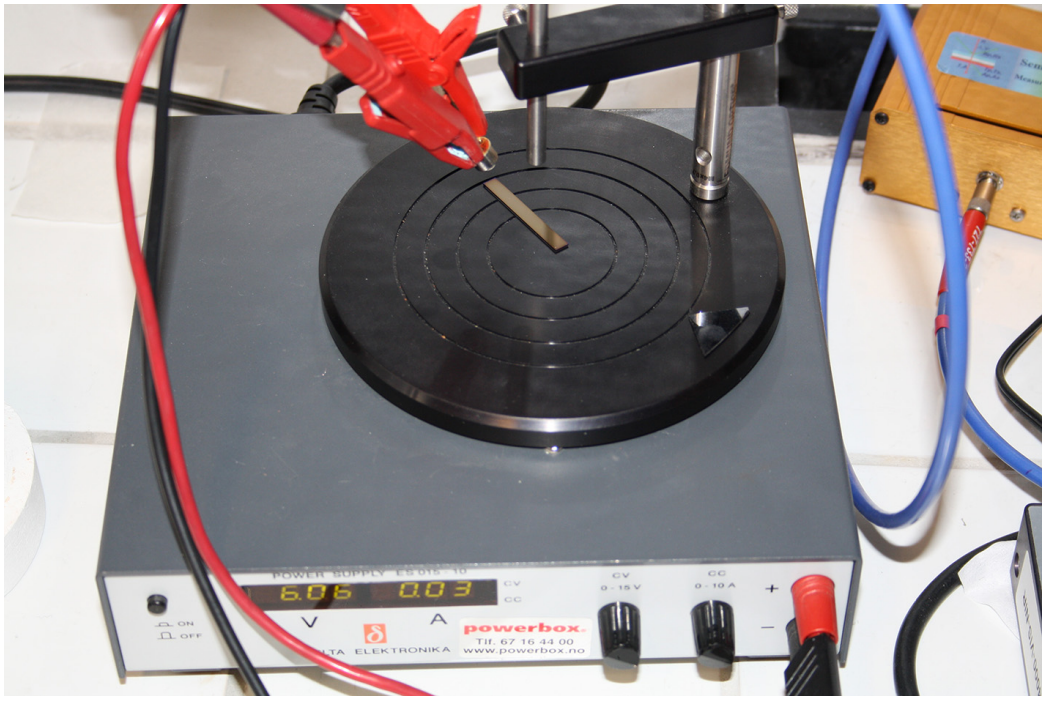

Figure 22: Setup of photo luminescence spectroscopy experiment.

3.12 Current-voltage characteristics

Current-voltage measurements used a pair of Keithley Sourcemeters, a 2400 and a 2635B, to control voltage and measure the current and log data. A small metallic lump of germanium added to the film surface while fluid functioned as an electrode contact on the thin film. A piece copper tape attached to the bottom of the stainless steel substrate functioned as the other electrode.

3.13 Reduction of samples

An ordinary tube furnace controlled using a Eurotherm 2132 temperature controller was used for reduction of samples.

Reduction in hydrogen atmosphere used a flow of 4% H_2 in argon from

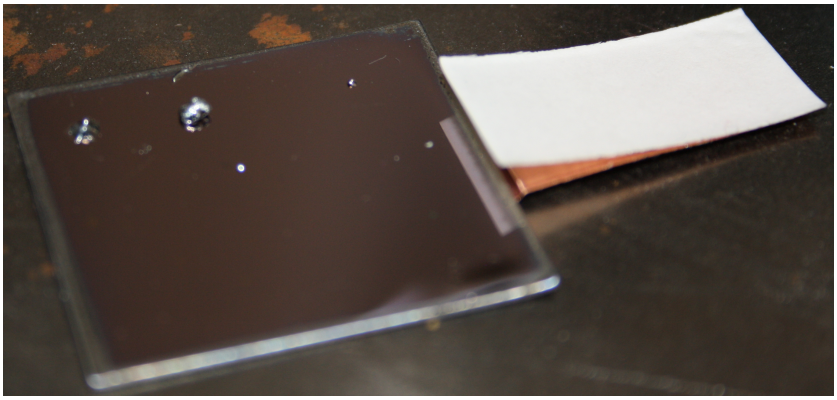

Figure 23: Sample preparation for current-voltage measurements. A small sample of germanium is put on top of the film and an electrode is positioned in contact with the germanium.

AGA.

4 Results

4.1 TiO_2:Tb

Thin films of TiO_2 deposited with ALD using $TiCl_4$ and water as precursors is a well studied system. The crystal structure for the films depends on the deposition temperature[11] and the films in this work were deposited at 300°C which resulted in the anatase phase of titania, figure 24. A large reflection just short of 33° stems from the (200) plane of the silicone wafers used as substrates.

Doping titanium oxide films with terbium in ALD involves depositing layers of terbium oxide between the layers of titania. Deposition of terbium oxide films by ALD have not been studied in depth. Though this is a rather more thorough investigation of terbium oxide films, it is by no means an exhaustive study of the $Tb(thd)_3$ + O_3 ALD system. QCM has not been used to study this process because using O_3 to burn off organic ligands causes temperature and pressure fluctuations that interfere with the QCM data.

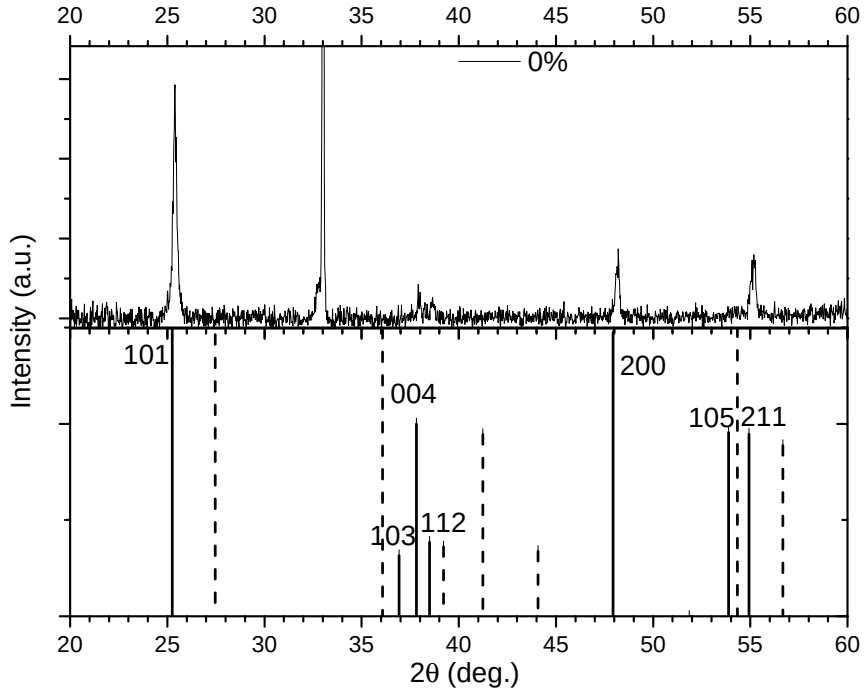

Figure 24: Top: diffractogram of the TiO_2 film. Bottom: reflections for the anatase (solid lines) and rutule (dashed lines) phases of titania. Labels show h k l of reflection planes of anatase.

The films containing terbium were deposited with pulse and purge time of 1.5 seconds for $Tb(thd)_3$. Initial depositions and the series with mixed titanium/terbium oxide were deposited with a 4 seconds O_3 pulse and 1.5 seconds purge. Some of the depositions from late in the project used reduced O_3 pulse times, primarily to check any effect on oxidation state.

As deposited terbium oxide films were characterized using XRD with the results displayed in figure 25. The crystal structure of the terbium oxide film has space group Fm-3m which means it can be Tb_2O_3, TbO_2 or Tb_4O_7.[40;41;42] As seen in figure 25 the unit cell size varies slightly for the different stoichiometry's and that the closest fit to the thin film diffractogram is the Tb_4O_7 morphology. This is an indication that conditions where $Tb(thd)_3$ reacts with ozone is too oxidizing to produce Tb_2O_3 films.

Initial analysis of the luminescence properties of the TiO_2:Tb films revealed

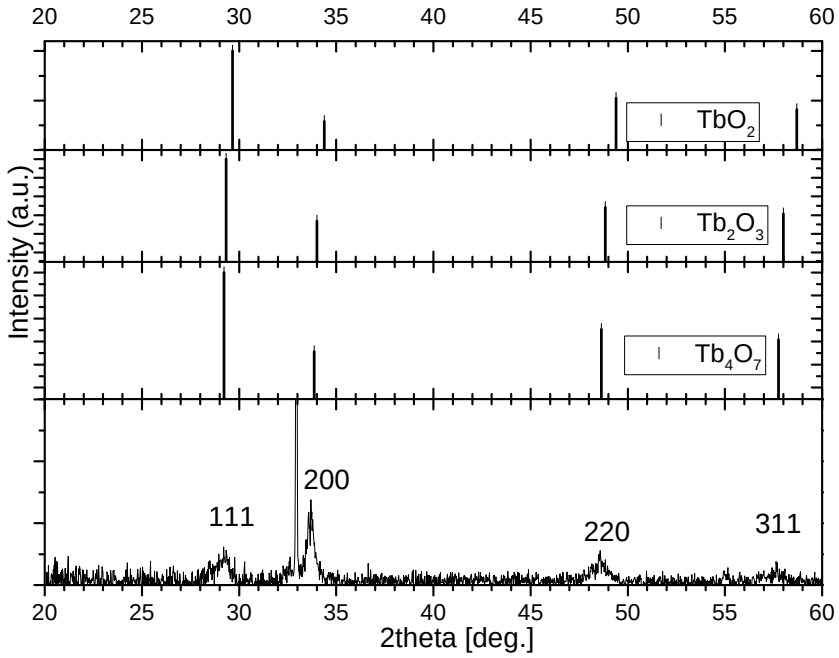

Figure 25: The powder diffraction peaks of TbO_2[40], Tb_2O_3[41] and Tb_4O_7[42] shown above the diffractogram of the as deposited terbium oxide film.

a lack of PL. Therefore the sample series was limited to six films that were deposited by varying the ratio of $TiCl_4$+H_2O and $Tb(thd)_3$+O_3 cycles. Making a series of TiO_2:Tb films that were the same thickness was not attempted.

XRD scans of the TiO_2:Tb films reveal information about the microstructure of the films. To make the reflection peaks stand out, and make comparison between the scan easier, the background level has been removed using EVA. Only the scan of films with pure titanium oxide, 5% $Tb(thd)_3$ cycles and pure terbium oxide have a clear crystal structure. The lack of reflections in the remaining samples indicates that they are almost completely amorphous.

When mixing together several elements or precursor pairs with ALD the growth rate is often reduced. This is also the case the terbium doped titania

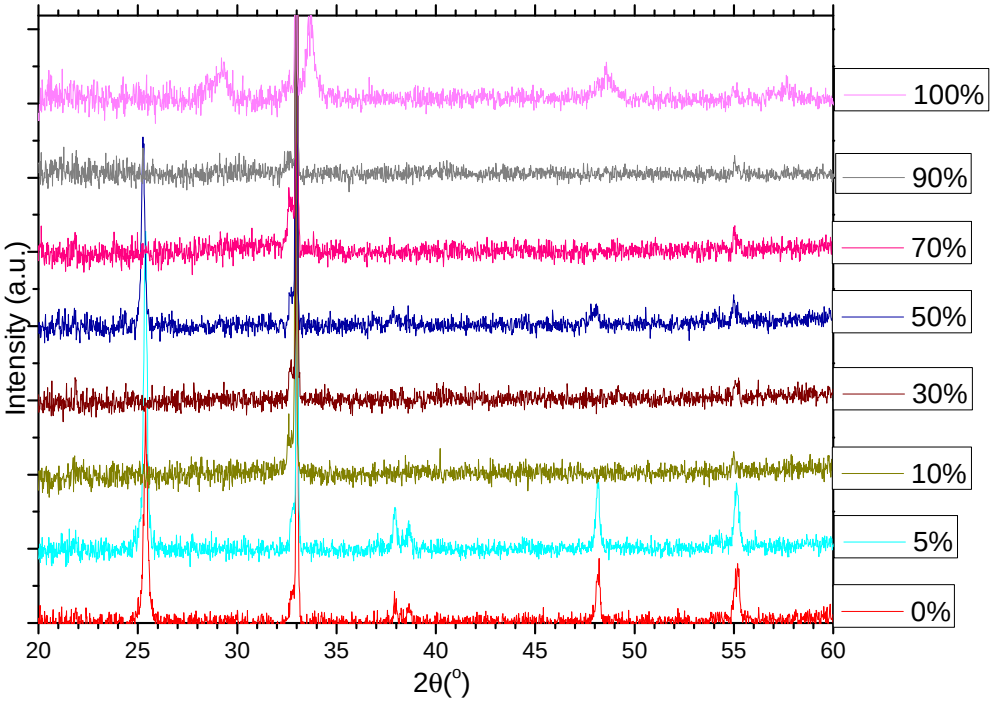

Figure 26: Diffractograms of the as deposited TiO_2:Tb film series.

films as seen in figure 27. The thickness of one of the samples, the front substrate of the 5% $Tb(thd)_3$ cycle sample, seems anomalously high. Very high growth rate may be indication of CVD growth due to both precursors being present in the reaction chamber simultaneously. Though this is probably the case for this sample the thickness of the other two substrates is close enough to the 0% and 10% $Tb(thd)_3$ cycles to be comparable. The anomalously thick front sample was not used in further characterization.

The "rule of mixtures" formula used to calculate theoretical growth rate for the mixed oxide films is equation 6.[43] Figure 27 shows clearly that the two ALD processes interfere with the growth of each other. The very steep slope from the 90% Tb cycle sample to the 100% Tb cycle is evidence that growth of terbium oxide is more hindered by the titanium cycle than vice versa.

$$\text{growth rate} = (0.78\text{Å/cycle})\%\text{Tb(thd)}_3 + (0.92\text{Å/cycle})(100 - \%\text{Tb(thd)}_3 \tag{6}$$

The sample deposited with 100% Tb(thd)_3 cycles in figure 27 was the result of experimentation with shortened ozone pulse. The purpose was the see if a shorter ozone pulse had any effect on the oxidation state of terbium. A pulse duration of 1 second and 1/2 second did not have any effect on the PL of the as deposited film. The film deposited with 1 second ozone pulse was approximately the same thickness as film deposited with 4 seconds ozone pulse.

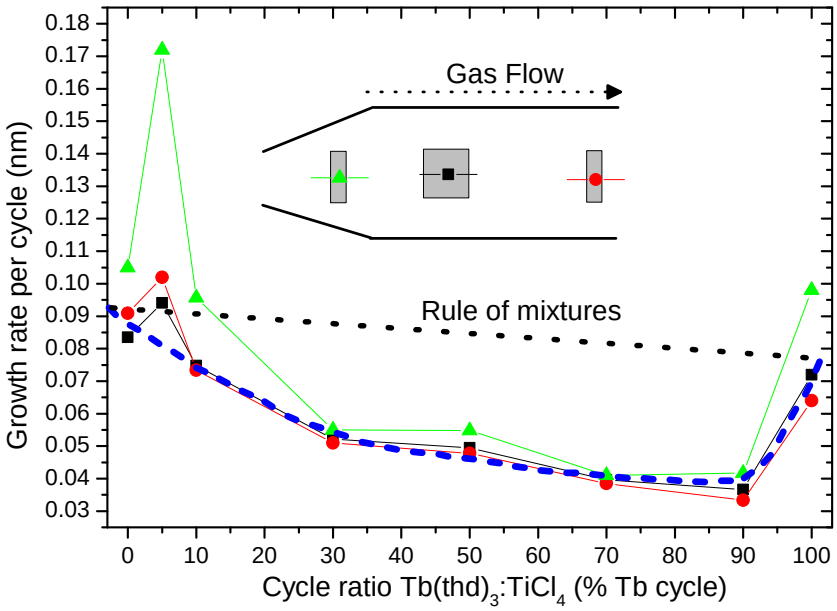

Figure 27: Growth rate of films from the TiO_2:Tb series as a function of percentage of Tb(thd)_3 cycles in the deposition. Dotted line shows thickness according to the rule of mixtures.

XRF was used to determine the terbium content of the titanium/terbium mixed oxide films. Terbium contents as a function of Tb(thd)_3 cycles is

shown in figure 28. Values in mole fractions of terbium oxide are calculated for Tbi_4O_7, but the data was analyzed for content of Tb_2O_3 and TbO_2 as well. The differences between the terbium content for the different oxides was so small that they were barely distinguishable on the graph and therefore left out. The quite low terbium content for the sample with 90% pulsed $Tb(thd)_3$ indicates that the reaction of the precursor on the substrate is impeded.

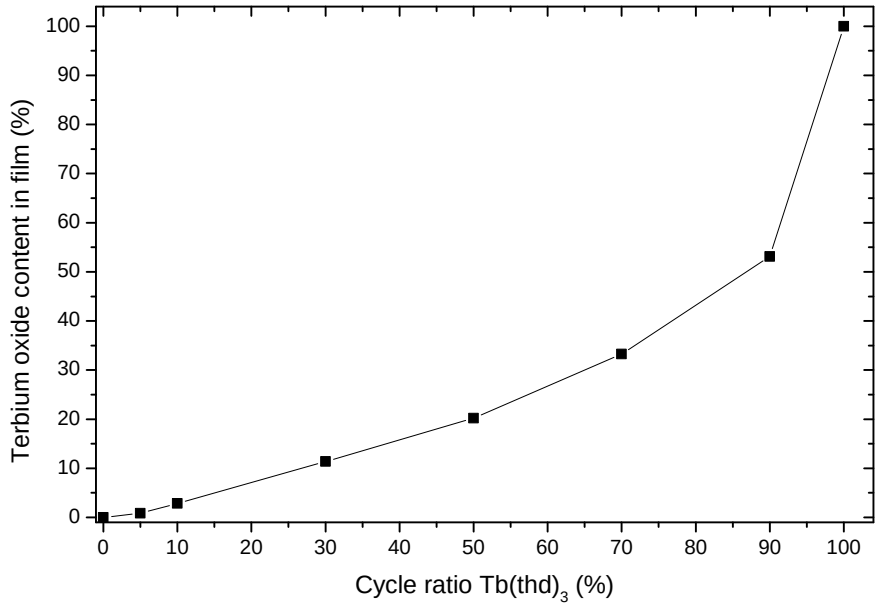

Figure 28: Terbium content of TiO_2:Tb films. Doping levels are in percentage of $Tb(thd)_3$ + O_3 cycles.

Optical properties of the mixed oxide films were investigated using UV/VIS spectroscopy on the terbium doped thin films using an integrating sphere. Transmission and reflection of thin films deposited on glass was measured and absorption was calculated. Measurements of a glass plate without any film was performed and used for reference for what wavelengths the glass influences the absorption.

It is obvious that the two films with highest terbium content have different absorption with a wide peak in the area around 400nm. This is probably caused by the charge transfer absorption which also give the material its

color as reported by Mccarthy.[44]

The films made with 10% and 30% terbium cycles have very similar spectra but quite different magnitude of absorption. There might be several wide absorption peaks behind the shape of the spectrum, one of which could be the same as the distinct wide peak in the visible range on the 5% film.

The 50% and 70% films have a very different absorption to the other films with no absorption in the visible spectrum and a distinct peak around 320nm for the 50% film and 280nm for the 70% film.

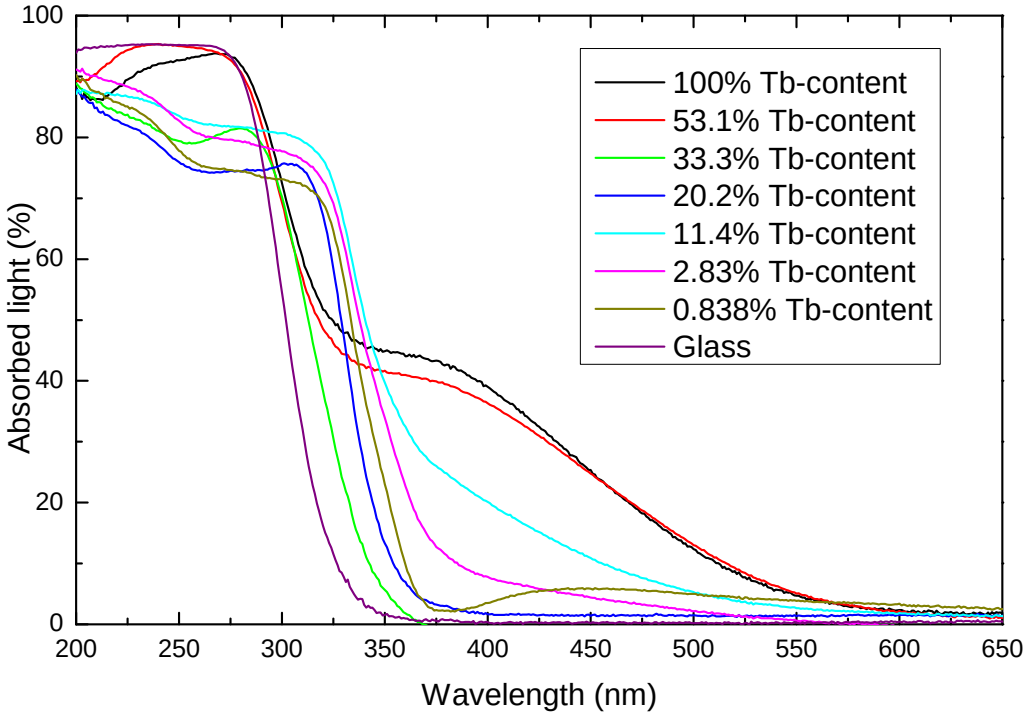

Figure 29: Absorption of the terbium/titanium mixed oxide films.

Investigation of the films luminescence properties are initially done using a UV-lamp and visually checking for PL. Results were negative for PL of the terbium/titanium mixed oxide films. Using a UV-laser to increase the energy of excitation radiation also resulted in absence of PL.

Lack of luminescence was assumed to be caused by oxidation of terbium(III)

during deposition. Attempts were therefore made to reduce terbium in the thin films in addition to a reference sample of terbium(III,IV) oxide powder by annealing under reducing conditions. Terbium(III,IV) oxide powder was annealed for 7 hours in a constant flow of H_2 gas changing the color of the powder from dark brown to pale brown (figure 30).

Figure 30: Terbium oxide powder before (left) and after (right) annealing in H_2 at 1200°C for 7 hours.

None of the terbium oxide thin films annealed in reducing conditions emitted PL under UV-light on visual inspection. Figure 31 shows the annealed films with an as deposited film for comparison. The samples used in annealing were deposited with shortened ozone pulses.

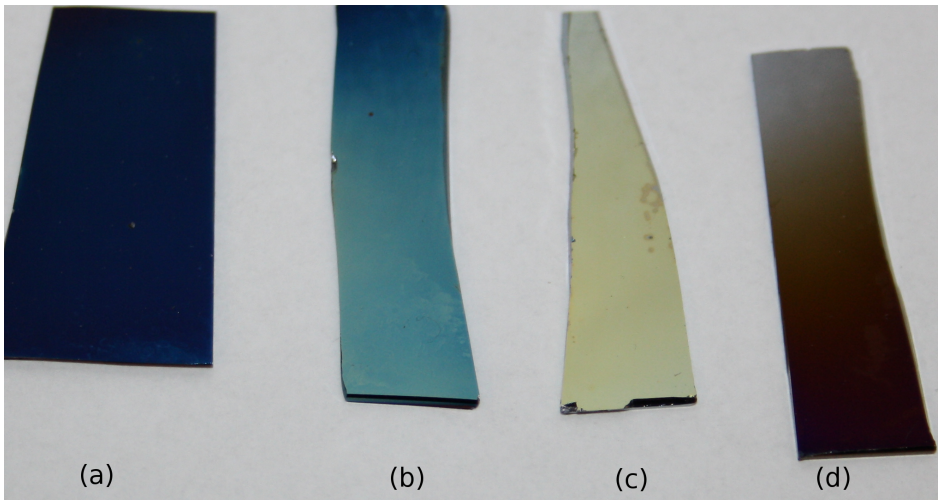

Figure 31: (a) As deposited film on silicon wafer. (b) Sample annealed at 1000°C in H_2 for a half hour. (c) Sample annealed at 1200° in H_2 for one hour. (d) Sample annealed in sealed evacuated ampule with oxygen getter at 1200°C for more than 8 hours.

XRD characterization of the thin film before and after annealing reveal a change in the crystal structure of the sample. Searches for a powder diffraction pattern matching the peaks of the annealed thin film were unsuccessful.

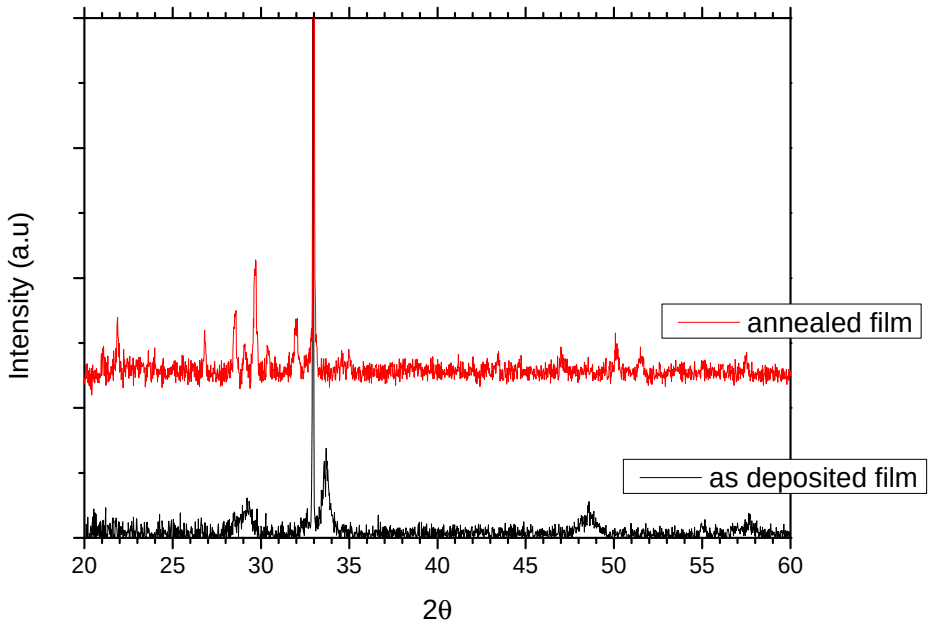

Figure 32: XRD diffractogram of terbium oxide film annealed in H_2 atmosphere at 1200°C.

4.2 Terbium(III) salts

When the titanium/terbium mixed oxide films proved absent PL, evidence was sought that terbium(III) compounds would be photo luminescent. The salts are: $Tb(SO_4)_3 \cdot 8\,H_2O$, TbF_3 $TbCl_3 \cdot 6\,H_2O$ and $Tb(NO_3)_3 \cdot 6\,H_2O$, plus the ALD precursor $Tb(thd)_3$. All of the salts and compounds were white powders with reflexibility comparable to $BaSO_4$ as seen in figure 34.

PL properties of the salts and the $Tb(thd)_3$ complex was investigated. Figure 33 shows the normalized PL as a function of wavelength of luminescence. All

of the samples were luminescent with the typical spectra of terbium(III). The fact that PL is present in the various terbium(III) salts and the precursor strongly indicate that any Tb^{3+} ions in the thin films should emit PL.

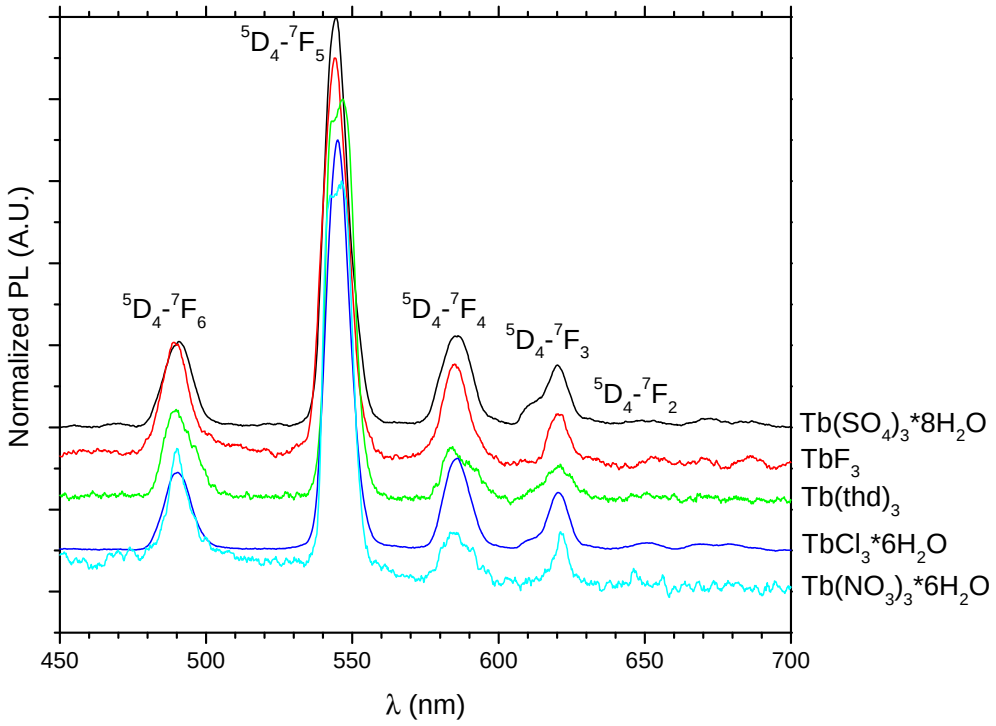

Figure 33: Photo luminescence as a function of wavelength for some terbium(III) salts and compounds. $Tb(thd)_3$ is the same as the precursor used in deposition.

Reflectance measurements of the salts and the $Tb(thd)_3$ precursor was performed on the equipment used to measure PL. A $BaSO_4$ reference sample, also used in UV/VIS spectroscopy, was used as reflectance standard. The sharp peak at $\lambda = 488$ nm is absorption from the $^7F_6$-$^5D_4$ transition. If electrons from an excited Tb^{3+} ions other ^7F-states relaxes to the free $^7F_6$ state, the relaxation from the $^5D_4$ state will result in emissions of longer wavelength. The generally poor quality of the graphs is because the PL equipment is not optimal when used for measuring reflection.

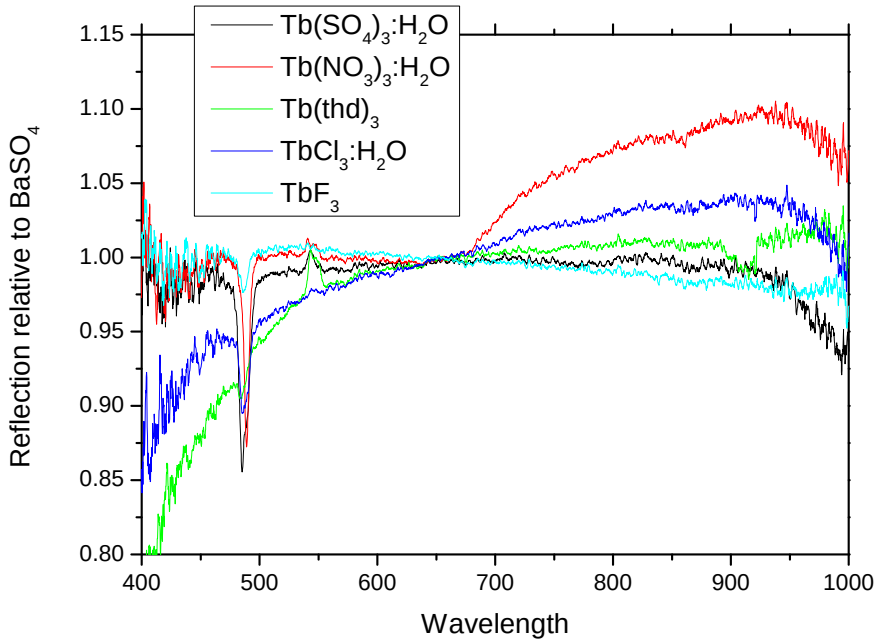

Figure 34: Diffuse reflection of terbium salts and the terbium precursor used in ALD as a function of wavelength. The reflection is relative to the reflection of a $BaSO_4$ standard.

4.3 Organic-inorganic hybrid films containing terbium

In order to maintain the oxidation level of terbium during deposition it became apparent that a different anion precursor than O_3 was needed. The most evident alternative to ozone would have been water. Previous attempts within the group with using water as anion for $Yt(thd)_3$ were unsuccessful and water was therefore rejected as a source of oxygen. A more reactive non-oxidizing reactant than water is a carboxylic acid. 1,4-bdc, a bi-functional carboxylic acid, was chosen as a reactant for $Tb(thd)_3$. This choice was based on prior experience within the group that 1,4-bdc could be reactive with thd-based precursors.

An initial test of deposition of terbium-hybrid film was performed using 1.5 seconds pulse and purge of $Tb(thd)_3$ and 2 seconds pulse and 1 second purge

of 1,4-bdc. The test used a deposition temperature of $T_d = 300°C$ and precursor temperatures of 145°C for $Tb(thd)_3$ and 200°C for 1,4-bdc. The ALD parameters were set based on past experience with each individual setting, either in this work or in other's work in the group. On visual inspection the resulting film was without thickness gradients and had good coverage over the entire substrate. The precursors also show sufficient sublimation and recrystallization which indicates a suitable flow of precursor into the reaction chamber.

Figure 35: Image of precursor tube with a boat containing precursor. During purging the precursor recrystallizes on the inside of the tube, called back sublimation.

An in situ QCM experiment was thereafter conducted with the aim of obtaining information on the growth process and suitable times for the pulsing and purging. Deposition temperature for the QCM experiment was $T_d = 250°C$. There are many phases in a QCM experiment to investigate different elements of the ALD process. Information regarding the growth rates dependency of different pulse and purge parameters are presented in figure 36. These were obtained by individually varying the pulse and purge parameters for sequences consisting of 20 cycles and monitoring their growth rate by QCM. A pulse duration of the $Tb(thd)_3$ precursor of about 1.5 to 2 seconds is sufficient for saturation of the substrate. Longer pulse times may increase the absorption slightly but does not have a significant effect on the growth rate of the film. The length of purge of Tb(thd)3 does not seem to have notable effect on the growth rate of the film, indicating that the sticking coefficient of the $Tb(thd)_3$ precursor is low.

A possible CVD growth is observed for the shortest purge times by an increased growth rate, indicating that the 1,4-bdc precursor sticks to the surface. For very long purge durations, the growth rates are reduced, possi-

bly due to release of adsorbed precursor or rearrangement of the precursors leading to loss of number of active sites for the subsequent $Tb(thd)_3$ precursor.

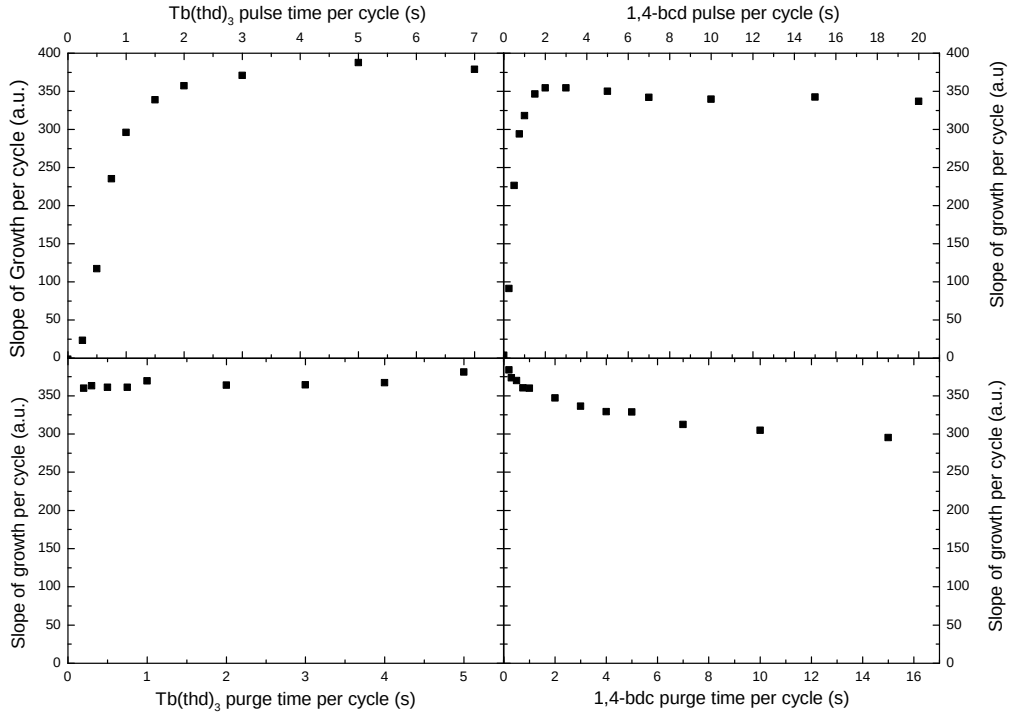

Figure 36: Graph with analysis of growth rate from QCM experiments with various duration of pulse and purge parameters of the precursors.

The dependency of growth rate with deposition temperature was investigated in the range 225-350°C, Figure 37. The growth rate is highest for the lowest deposition temperatures and decreases linearly up to 300°C before remaining nearly constant between 300 and 350°C.

The in situ QCM allowed investigation of the variations in mass during one cycle somewhat more detailed. A relatively long pulse sequence consisting of 7s $Tb(thd)_3$ pulse, 5 s purge, 20 s 1,4-bdc pulse, and 15 s purge, was cycled for 20 times. The 16 middle cycles were averaged to obtain better counting statistics and is presented in Figure 38.

The mass of the film increases significantly during the $Tb(thd)_3$ pulse and

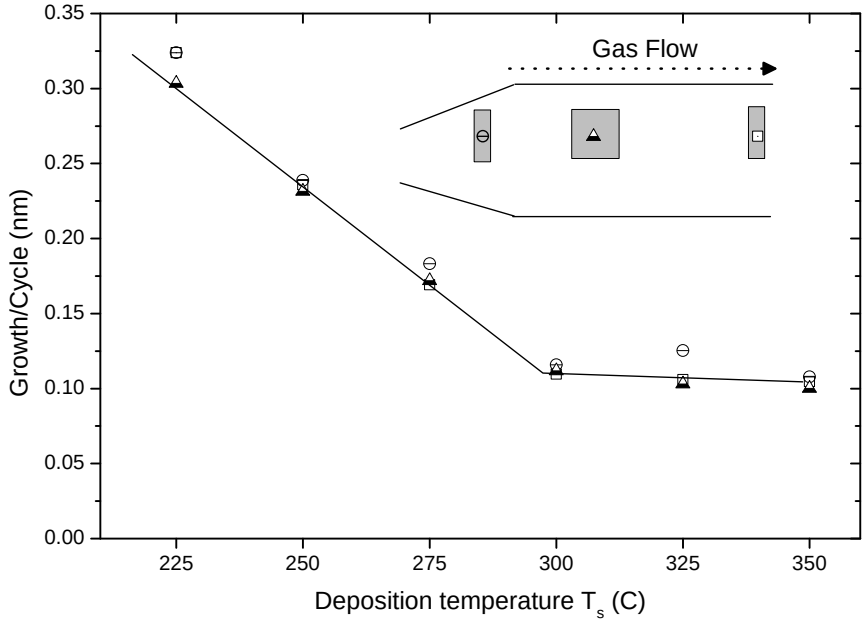

Figure 37: Growth rate of Tb-hybrid films deposited at temperatures ranging from 225°C to 350°C. The inset figure shows the configuration of the samples in the reaction chamber.

reduces somewhat when 1,4-bdc is pulsed, reflecting the difference in mass between the thd and 1,4-bdc molecules. The change in mass during 1,4-bdc pulse and purge amounts to a reduction of about 28.8% of the mass increased during $Tb(thd)_3$ pulse and purge.

The ratio of frequency change during a cycle is the same as the ratio of mass change during a cycle: $\frac{\Delta f_b}{\Delta f_a} = \frac{\Delta m_b}{\Delta m_a}$. Assuming an overall stoichiometry of Tb_2(1,4-bdc)$_3$ the following reactions occur on the substrate:
$(RCOOH)_x$ + $Tb(thd)_3$(g) $\rightarrow$ $(RCOO)_3Tb(thd)_{3-x}$ + xHthd(g)
$(RCOO)_xTb(thd)_{3-x}$ + 1.5 RCCOH(g) $\rightarrow$ $(RCOO)_{1.5}$Tb + (3-x)Hthd(g)
The mass balance of the reaction is given by:

$$\left(m_{Tb(thd)_3} - x m_{Hthd}\right) 0.288 = 1.5 m_{1,4-bdc} - (3-x)\, m_{Hthd} \qquad (7)$$

where $\Delta m_a = m_{Tb(thd)_3} - x m_{Hthd}$ and $\Delta m_b = 1.5 m_{1,4-bdc} - (3-x)\, m_{Hthd}$.

Molecule	*Molar mass*
Hthd	184.28 g/mol
1,4-bdc	166.13 g/mol
$Tb(thd)_3$	708.74 g/mol

Table 2: Molar mass of the precursors and the thd ligand.

Solving for x results in:

$$x = \frac{1.5m_{1,4-bdc} - 3m_{Hthd} - 0.288m_{Tb(thd)_3}}{-1.288m_{Hthd}} = 2.15 \tag{8}$$

The solution to equation 7 shows a reaction mechanism where $Tb(thd)_3$ releases two Hthd on reaction with the substrate and the remaining ligand is released during the 1,4-bdc pulse.

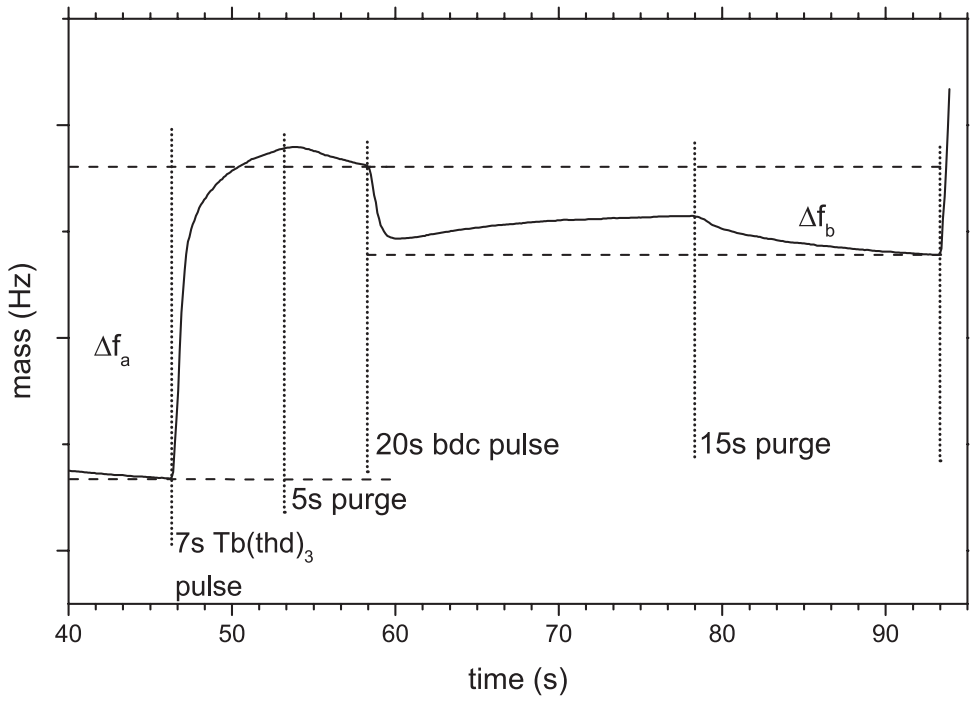

Figure 38: QCM long cycle data. The four stages of the cycle are marked with dotted lines and the length in seconds of each pulse and purge is written. Δf_a is mass increase during pulsing and purging of $Tb(thd)_3$, Δf_b is mass decrease during purging and pulsing of 1,4-bdc.

The initial steps of any ALD deposition involve adsorption and reaction on bare substrates. The first cycles of the QCM experiment deposits films on the bare gold electrodes of the sensor. These surfaces may have a notably lower density of potentially active sites than an oxide surface.

By monitoring the mass increase from the first cycles of the deposition, it is evident that this is negligent, but gradually increases during the first 10 cycles. The low initial growth rate is due to limited nucleation on the gold surfaces of the QCM crystal. After the initial buildup of film on the crystal the growth follows a linear slope.

A similar experiment was also conducted later in the experiment when the film was deposited on native hybrid film. This shows no sign of inhibition period due to the long purging period of 30 s before deposition resumes.

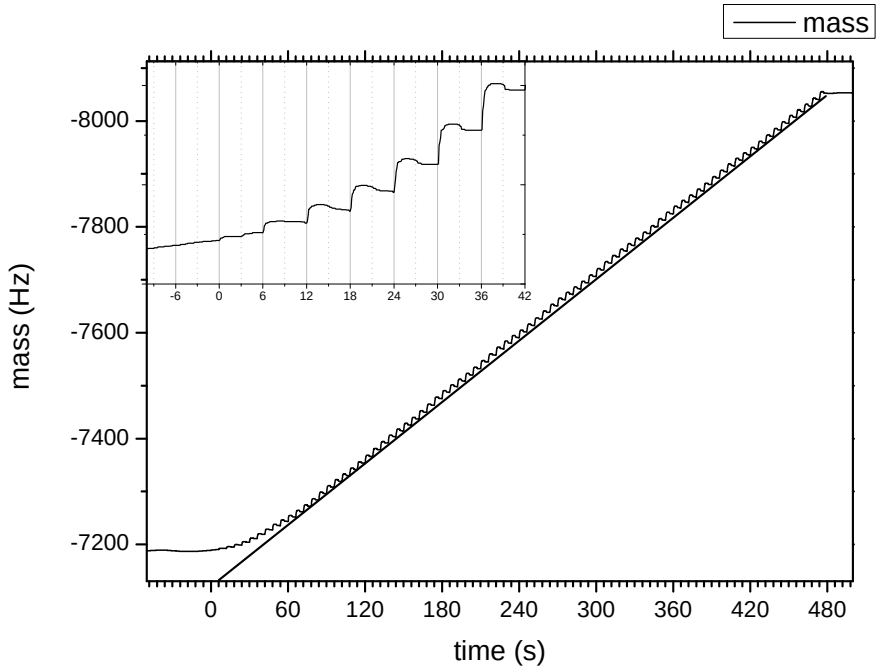

Figure 39: Graph shows the first 80 cycles of ALD deposition on the quartz crystal. Inset is the start of the deposition on the gold surface with major grid lines when $Tb(thd)_3$ is pulsed and minor grid lines when 1,4-bdc is pulsed.

Figure 40 shows a 30 second pause in the deposition, 40 cycles of film deposition and ends in a 30 second pause. The transition between the pause and the deposition phases indicates that the deposition requires no new nucleation to resume normal reaction after the pause in the cycle. This phase of the QCM experiment and the first nucleation phase both have the same pulse and purge lengths as the temperature series: 1.5s, 1.5s, 2s, 1s.

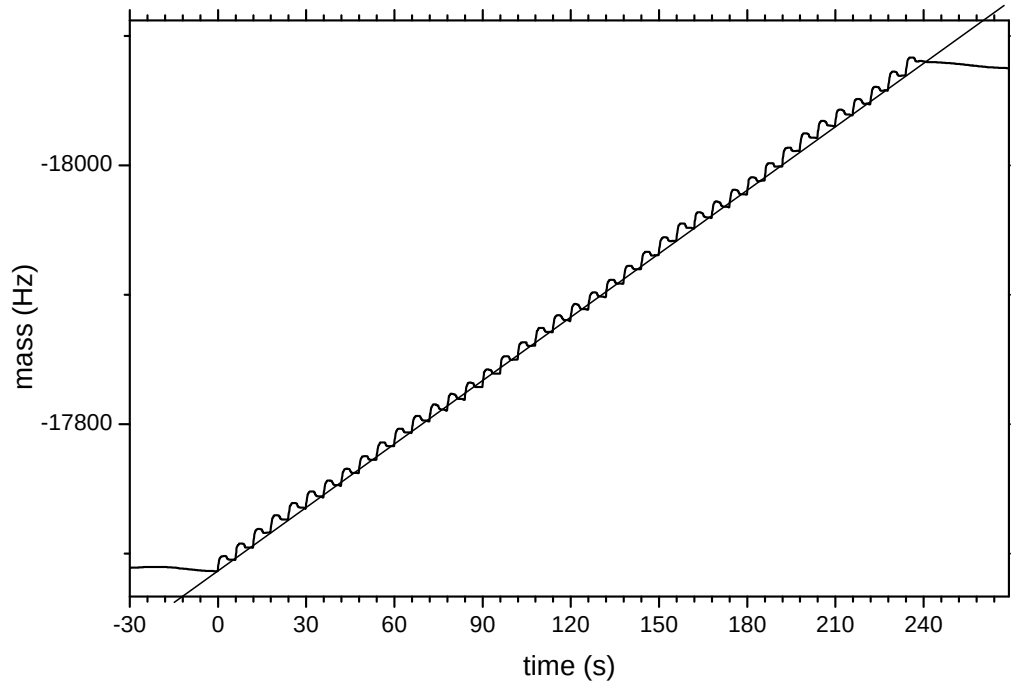

Figure 40: QCM data showing the change in mass during ALD deposition.

A larger number of cycles were used for investigation of the stability of the deposition, Figure 41. The linearity phase is 300 cycles long and lengths of pulse and purge are slightly different than for 40 and 39. A linear regression was using the data from the linearity run, and the r^2 value for the fitted linear function was 0.99997.

The chemistry of the films was investigated using FTIR analysis. Two scans of the same sample, one directly after deposition and the other 16 days later, were performed to check the stability of the films after extraction from the reactors. Both scans lack the obvious signs of the stretching associated with

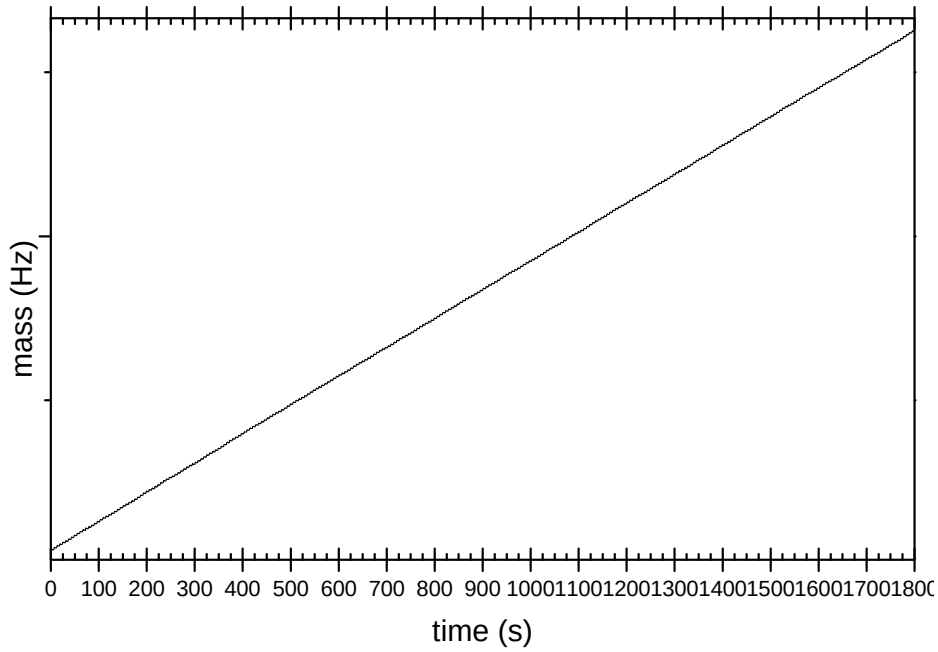

Figure 41: QCM data showing the linearity phase of the QCM experiment. The pulse and purge parameters for the linearity phase are slightly different from the parameters of thin films produced in this work.

residual OH-groups in the film. In some cases organic-inorganic hybrid films absorb water from the atmosphere and recrystallize over time.[21] This does not seem to be the case for the terbium-hybrid film, though weather conditions and humidity may be contributing factors that are difficult to replicate.

The peaks from the carboxylate groups are at 1544 cm^{-1} for the asymmetric and 1392 cm^{-1} for the symmetric stretching modes. The separation of stretching modes of 153 cm^{-1}cm indicate a bridging complex, where the carboxylate group stretches between two terbium ions.

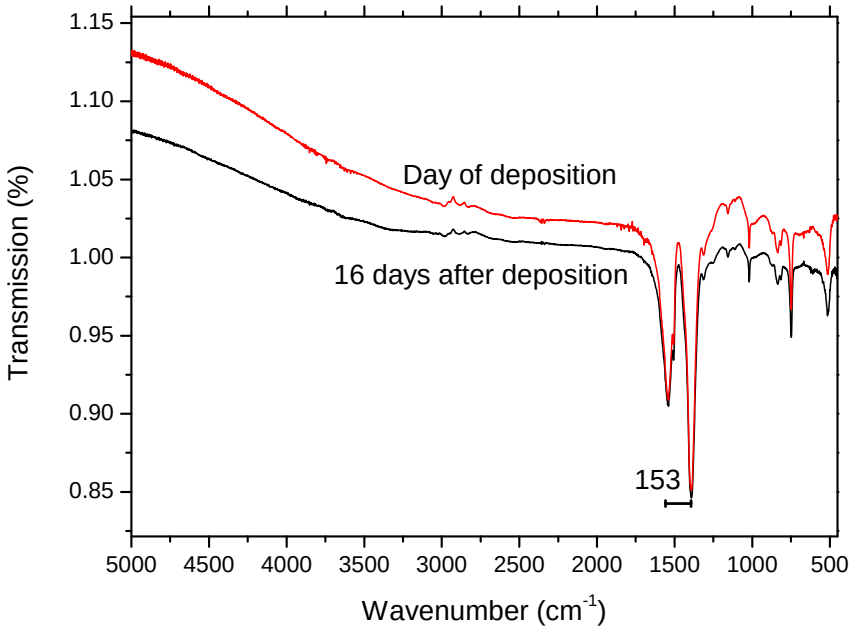

Figure 42: FTIR of same Tb-hybrid film taken at different time intervals after exposure to air. The first scan was taken shortly after exposure, while the second was taken 6 days later.

Though the FTIR data in figure 42 does not indicate that the film absorbs water from the atmosphere, there does seem to be some changes in the film after it is deposited. This is evident from the slight changes in thickness of the film in the time after it was deposited shown in figure 43. The first measurement was performed directly after extraction from the reactor. The next three were performed later the same day at one hour intervals. The final measurement was performed 3 day later.

Investigations into whether the increase in thickness could be an artifact of ellipsometry measurements were done without conclusive evidence that this is the case. This information is found in appendix B. The cause or nature of the process causing the film to get thicker after deposition is not known.

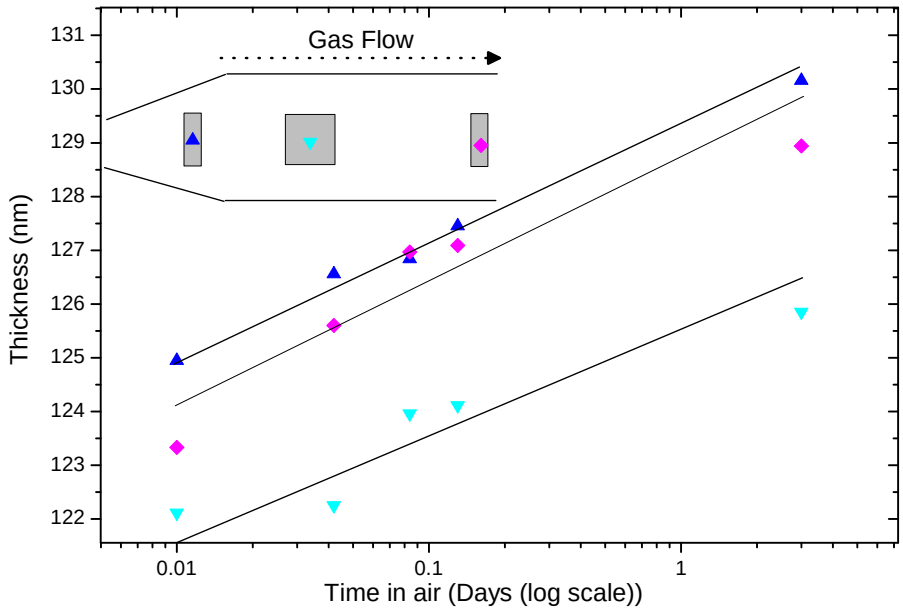

Figure 43: Plot showing the thickness of the film measured right after extraction from the reactor and at increasing intervals. The scale of the x-axis is logarithmic to separate the measurements in the graph.

Optical properties of the terbium-hybrid films was performed with UV/VIS spectroscopy. The terbium hybrid films are transparent to visible light as seen from the UV/VIS measurements in figure 44. There were some difficulties with masking around the sample due to the shape and size of the sample and the sample holders on the integrating sphere. This is may explain the higher absorption of the 19nm film in the visible region of the spectrum, as it is difficult to think of a mechanism for the 19 nm film to absorb more light in the visible spectrum than the 124 nm film. A consequence of this error is absorption of the 124nm film around the $\lambda = 250$ is likely near 100%.

For comparison to other hybrid films the UV/VIS scan of a cobalt hybrid thin film performed by another student in the group is included in figure 44. Though the intensity of absorption of the terbium and cobalt hybrid films are different, the pattern of the scan shows similarities that indicate that absorptions are due to the organic molecules, not the cations.

There are several interesting similarities in the UV/VIS data. All three films show a dip in absorption around λ=220 nm, even though it seem like the 19 nm terbium hybrid film the dip is shifted slightly to λ=225 nm. All three films have a broad maximum peak in absorption centered around λ=250 nm. The terbium hybrid films have a very clear shoulder on the right side of the large maximum peak, with a hint of a cusp on the data for the 19 nm film at λ=280 nm. There is also a hint of a large round shoulder on the cobalt hybrid films, but the much larger size of the maximum peak obscures it significantly.

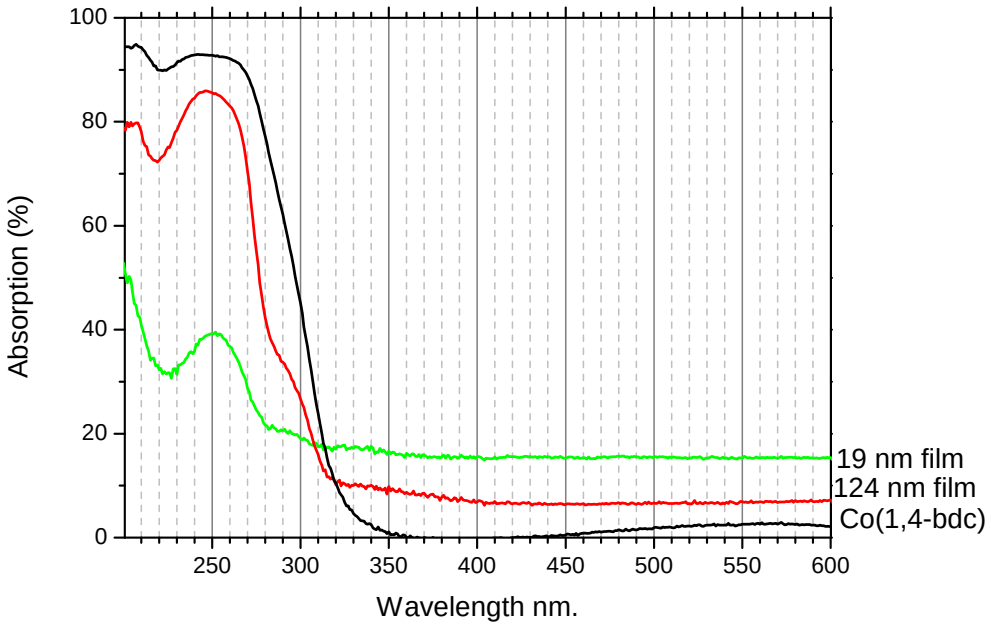

Figure 44: UV/VIS light absorption of terbium-hybrid thin films. The lower absorption of the 124 nm film vs the 19 nm film is most likely due to difficulties light leaking around the edges of the substrate of the 124 nm film. The Co-1,4-bdc graph shows the absorption of an organic-inorganic hybrid film containing cobalt rather than terbium in order to compare absorption mechanism.

PL measurements were performed with a light emitting diode as source of

excitation energy. The setup was kept as similar as possible with regards to the distance from UV-source to sample, distance from sample to sensor and measuring samples of identical size and shape to make comparisons of relative intensity possible. Figure 45 shows the PL results of the PL measurements with the same scale for all three graphs.

Luminescence from the thinnest film seems to be limited to the most intense wavelengths of light emitted from Tb^{3+} ions. The 3 medium medium sized peaks shown clearly on the graph from the thickest film is missing completely from the 19nm thin film. The 86nm film data does show four of the five peaks typical of Tb^{3+} luminescence, though the peaks with lowest intensity barely rise above the noise. The 152nm film has an order of magnitude higher intensity than the thinnest film, and about a factor of four higher intensity than the 86nm film. The lowest intensity light emitted at around $\lambda = 650$ nm is barely above the level of the noise.

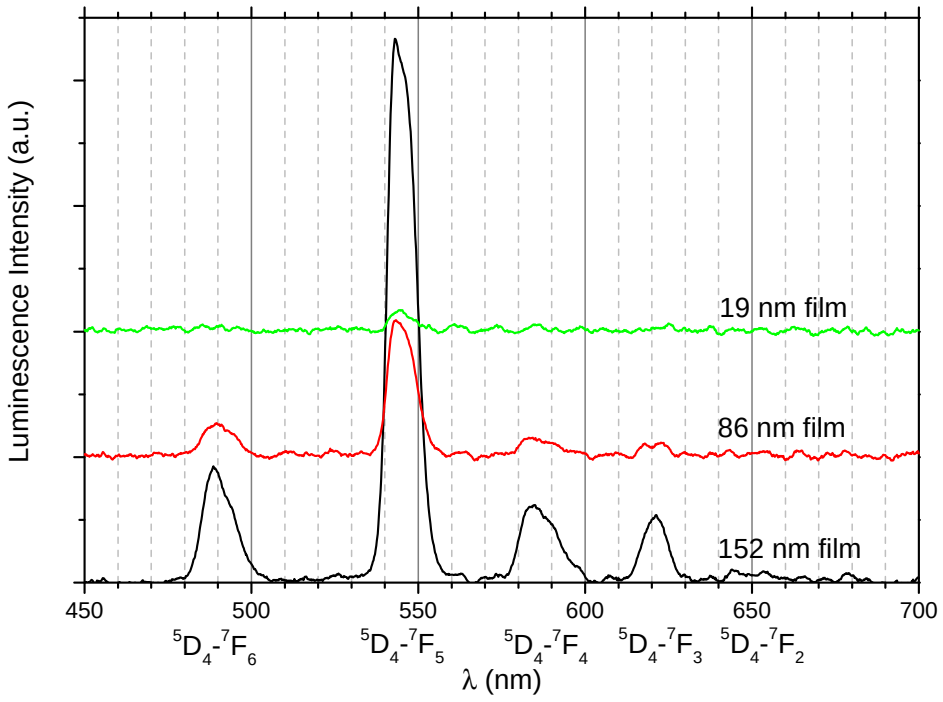

Figure 45: Photoluminescence measurements of terbium-hybrid thin films.

The electrical properties of as-deposited films were also investigated using a two electrode approach. The overall conductivity of the samples were expected to be so low that any contact resistance would be negligible. The measurements were performed on films deposited on steel substrates to determine the resistance of the material. A total of 10 measurements were performed with a maximum voltage of each measurement of 1V up to 10V. The measurements with a maximum voltage of 1V and 2V are shown in figure 46 because they are the results with hysteresis behavior. Currents in excess of instrument tolerance were measured for maximum voltages of 3V and above. This type of voltage-current characteristics are associated with ferroelectric materials.

The spikes in both graphs in figure 46 are also found in measurements performed on measurements performed by other students with the same equipment. The origin of the spikes is unknown but the positions seem to be unrelated to the voltage but rather related to specific instrument settings.

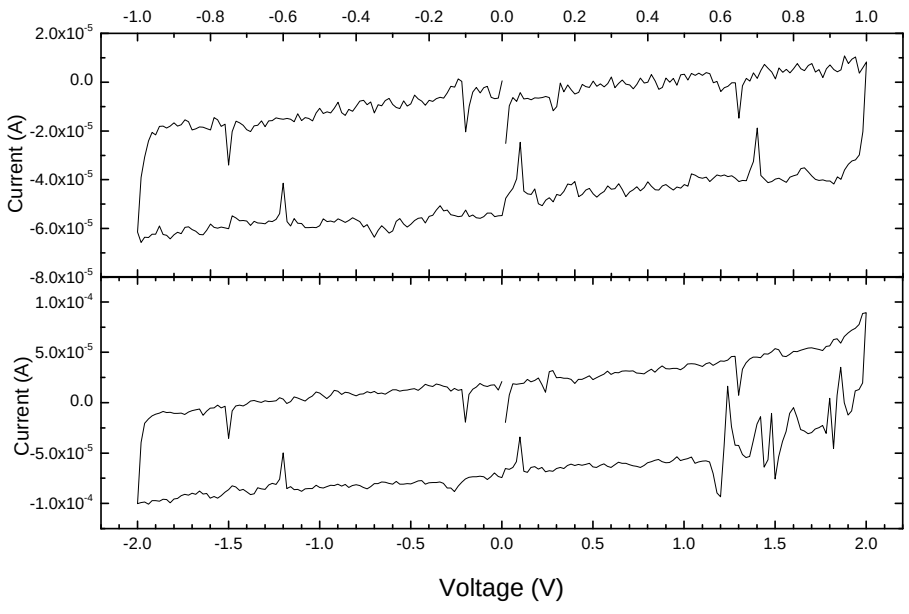

Figure 46: Current/voltage plot showing hysteresis curve of $Tb(bdc)_3$ film on steel substrate. The graph only contains data for electrical measurements for maximum voltage of 1V and 2V.

5 Discussion

The main focus of this work evolved during the project. The biggest challenge turned out to be maintaining the oxidation state of Tb(III) due to oxidation from O_3. Alternative anion precursors were required in order to preserve the luminescence properties observed in the $Tb(thd)_3$ precursor. The discussion is therefore divided into an inorganic and organic-inorganic hybrid section.

5.1 Inorganic terbium films

The luminescent terbium oxide nano-particles reported by Wakefield et al.[45] indicate that luminescent thin films of terbium oxide also should be possible. Terbium(III) oxide thin films have been synthesized by Andreeva et al., using reactive evaporation in oxygen, producing films with a white appearance.[42] Annealing the films at 500°C resulted in a change in color from white to brown and change in structure to Tb_4O_7. The description of brown colored films seems similar to the as deposited terbium oxide films in this work. Difficulty with maintaining oxidation state of Tb^{3+}, which over time oxidizes in air, has also been reported by McCarthy.[44] It is therefore not exceptional that using ozone as oxygen precursor in ALD fails to maintain the oxidation state of Tb^{3+}.

This work is not the first example of photoluminescent thin films deposited with ALD. Terbium, in the form of $Tb(thd)_3$ as precursors for ALD, has previously been used to produce photoluminescent and electroluminescent thin films.[8;9] These studies make use of $Zn(CH_3COO)_2$ as zinc precursor. The anions used were hydrogen sulfide as sulphur precursor and water as oxygen precursor. The zinc oxide films had a growth rate of one fifth of the sulphide films, and only the zinc sulphide films were doped with Tb^{3+}. Specific information about the ALD process involving doping the zinc sulphide films with terbium is not found in the article.

When depositing titanium/terbium oxide films, growth of the terbium oxide

layers seems to be severely hindered by the layers of titanium oxide. The film deposited with 90% $TiCl_4$ + H_2O cycles contains about 97% titanium oxide, while the film deposited with 90% $Tb(thd)_3$ + O_3 cycles only contains about 53% terbium. A likely explanation is that there are species on the surface after the titanium cycles that hinder terbium oxide nucleation.

The Aarik et al.[12] study of the $TiCl_4$ + H_2O reactions reveal a high concentration of chlorine for deposition temperature $T_d = 300°C$. Either chlorine is adsorbed onto the substrate, or volatile $Ti(OH)_xCl_{4-x}$ is formed on the surface during the deposition of titanium oxide layers. It is difficult to imagine a reaction mechanism between the thd ligands and the chlorine on the surface. Deposition of the titanium/terbium mixed oxides at higher temperatures might have provided much more information about the reaction mechanisms. The reasoning behind this is that the concentration of chlorine drops for higher deposition temperatures. If the chloride species on the surface are a hindrance to growth for terbium oxide, the growth rate would be expected to increase for deposition temperatures where little or no chlorine resides on the surface.

The decision to not use water as anion precursor was based on experiments with other similar processes which had been unsuccessful. Any use of water as precursor for terbium oxide at $T_d = 300°C$, when mixing the titanium and terbium processes, would probably also have failed because of the chlorine species present at that deposition temperature. With a higher deposition temperature more hydroxide groups would have been available on the surface. A higher temperature might also provide a change in the kinetics that allowed the reaction between hydroxide and the $Tb(thd)_3$ precursor.

Reduction of Tb^{4+} requires a temperature of 1300°C.[44] Attempts at reduction with H_2 gas or with zircon as oxygen getter at 1200°C were unsuccessful. A reducing agent strong enough to reduce terbium in situ might also cause damage to the ALD reactor and was not attempted. Reduction of Tb_4O_7 films is not a viable method of producing luminescent terbium oxide thin films.

This work has provided an explanation for why terbium oxide thin films and titanium/terbium mixed oxide films lacked luminescence. The search for anion precursor to react with the $Tb(thd)_3$ precursor included preparations toward producing TbF_3 thin films. Thin films of fluorides have previously been deposited by Pilvi et al. with thd-based precursors using TiF_4 as anion precursor. When a test using 1,4-bdc as anion resulted in luminescent thin films, the preparation were abandoned and the work focused on the inorganic-organic hybrid thin films.

5.2 Organic-inorganic hybrid thin film with terbium

Organic-inorganic hybrid thin films are fairly new in terms of ALD with the first article published in 2003. Only 8 articles are found using a carboxylic acid as precursor and two articles are found using 1,4-bdc. Hybrid thin films with the 1,4-bdc precursor have previously been deposited using aluminium, zinc and titanium as cations.[46;15] In addition another student in the group has deposited hybrid films using $Co(thd)_2$ and $Mn(thd)_3$ as cation precursors.

Figure 47 shows photos of what the initial inspection for PL looks like on as deposited films. Notice the non-luminescent areas on the glass plates where the silicone substrates block film growth. The photos also shows the much higher intensity of luminescence when the films are irradiated with light with $\lambda = 254$ nm. This is caused by the strong absorption of light in that area of the UV-spectrum shown in figure 44.

The growth rate as a function of deposition temperature of the terbium hybrid films shows a quasi-ald-window shape. A similar appearance has previously been reported by Klepper et al.[15] for the Al-1,4-bdc system. The area of near constant growth rate in this work even more pronounced that what is presented by Klepper. Klepper interpreted that the decrease in growth rate from 225-300°C was due to increased steric stress from thermal vibrations on the "dangling" ligands. This is likely also the case for the Tb-1,4-bdc system.

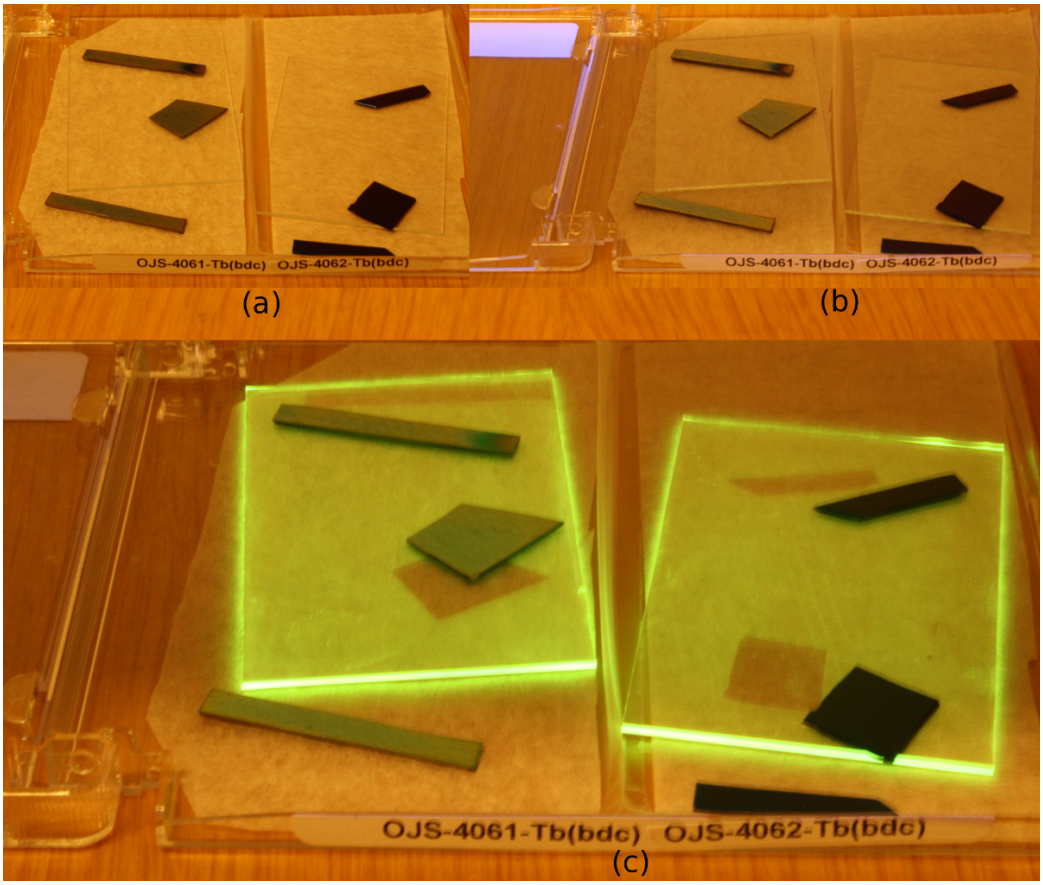

Figure 47: Photo of two samples $Tb_2(1,4\text{-bdc})_3$ thin films under (a) normal fluorescent light. (b) UV-light with $\lambda = 366$ nm. (c) UV-light with $\lambda = 254$ nm.

Intensity of luminescence measured in figure 45 and the absorption of light in figure 44 show results from films of different thickness. Comparing the relative intensity of absorption and PL shows that increase in PL for increased thickness is much greater than increased absorption for increased thickness. This leads to the conclusion that the lower absorption due to thickness of films is not the largest limiting factor for the films luminescence intensity. The increased number of luminescence emitters in the thicker films contribute more to the increased luminescence intensity than increased absorption.

The FTIR experiments in figure 42 show separation of the stretching modes that indicate reaction mechanisms dominated by bridging complexes. A sep-

aration of the peaks of $\Delta = 50 - 150$ cm^{-1} indicates a bidentate complex, $\Delta > 200$ cm^{-1} unidentate and $\Delta = 130 - 200$ cm^{-1} indicates bridging complexes.[15] The 153 cm^{-1} separation shown in figure 42 may be due to formation of mostly bridging complexes. A slight tick on the asymmetric peak and the shoulder on the symmetric peak could also be splitting of the peaks indicating the presence of both bidentate and bridging complexes.

The analysis of the terbium salts revealed a small but clear absorption peak at $\lambda = 488$ nm when compared to the $BaSO_4$ standard. In contrast there is no hint of absorption in the UV/VIS data for the terbium hybrid films. This might indicate that the thin films, which from XRD scans show no crystallinity, have fairly low terbium content. The high absorption around 250 nm could be a combination of the 1,4-bdc and the terbium absorption utilized in fluorescent lighting.

There was an extra signal in the QCM data of sinusoidal nature. Attempts at filtering the signal out resulted in more noise in the QCM data and were dropped. An analysis of how much the signal affected the mass calculations was performed and used in the analysis growth mechanism. This analysis can be found in appendix A.

A increase in thickness of the films was observed in the time after extraction from the reactor. The films FTIR scans did not show a marked increase in OH-stretching in the scans taken 6 days apart. Ellipsometry measurements taken over the whole surface of the samples revealed difference in thickness of comparable size to the increase in thickness. Later repetition of these measurements maintained the impression that the films increased in thickness in air. Data from these measurements can be found in appendix B.

6 Conclusions and future work

Terbium oxide thin films have been deposited with ALD using $Tb(thd)_3 + O_3$ as precursors. Use of O_3 to burn away the organic thd-ligands has proven to be too oxidizing to maintain oxidation state of terbium. In order to deposit terbium(III) oxide with ALD, different precursors need to be found that are able to maintain oxidation state of terbium to Tb^{3+}.

ALD has been used to deposit titanium oxide doped with terbium, with doping levels of 0.84%, 2.8%, 11%, 20%, 33% and 53%. This is a method of depositing thin films that allows a high degree of control the thickness of thin films. The resulting films are usually without thickness gradients and pinholes. Mixing different elements and molecules into a single film with a high degree of accuracy, and also with low risk of agglomeration of doped species, makes the method well suited for doping in thin films. Additional work investigating how deposition temperature changes the growth rate and perhaps the crystallization, and whether the reactions are possible using only water as anion precursor, is needed.

Characterization of the mixed oxide thin films using XRD shows a low level of crystallinity for mixed oxide films. An exception is the thin film with less than 1% terbium content which crystallized in the expected titanium oxide anatase structure. The structure of the terbium oxide film annealed under reducing conditions remained unknown. Perhaps due to reactions with pollutants in the H_2 gas, the substrate or remaining molecules from the deposition.

Optical properties of the titanium/terbium mixed oxide thin films, measured with UV/VIS, show they are dependant on terbium content. The total absence of absorption due to the characteristic spectrum of Tb^{3+} confirms that terbium was oxidized during deposition.

The thickness of the TiO_3:Tb films, measured with ellipsometry, show a large deviation from the "law of mixtures" and indicate hindered growth during the terbium cycles of the deposition. The hindrance can be investigated by varying the deposition temperatures and pulse/purge parameters and investi-

gating the change in growth rate. Since the $TiCl_4$ + H_2O system is very well studied, the remaining species on the substrate are known. Finding a deposition temperature where the species most likely to react with the $Tb(thd)_3$ precursor might be possible with more experimentation.

The growth of the Tb-1,4-bdc thin films follows the pattern reported by Klepper et al. with decreasing growth rate for increasing temperature.[15] The stretching modes found from FTIR scans are dominated by bridging of the carboxylate group between two terbium atoms. The growth mechanism investigated by QCM supports an overall stoichiometry of Tb_2(1,4-bdc)$_3$.

Investigation of the voltage-current characteristics of the hybrid film resulted in hysteresis-like shape to the graphs at voltages of 1V and 2V. Further investigations, if possible of both bulk material and thin films, can determine the mechanism behind these characteristics.

After extraction from the reactors, while the samples lay in air, the thickness of the films increased. A thorough investigation into the chemical and structural properties, and how these change with time, of the films will determine the stability of the hybrid films.

References

[1] A. B. Arons and M. B. Peppard. Einstein's proposal of the photon concept—a translation of the annalen der physik paper of 1905. *American Journal of Physics*, 33(5):367–374, 1965.

[2] Bernard Valeur. A Brief History of Fluorescence and Phosphorescence before the Emergence of Quantum Theory. *Journal of Chemical Education*, 2011.

[3] E.N. Harvey. *History of Luminescence from the Earliest Times Until 1900*. Memoirs Series. American Philosophical Society, 1980.

[4] G. G. Stokes. On the change of refrangibility of light. *Philosophical Transactions of the Royal Society of London*, 142:pp. 463–562, 1852.

[5] Ulises Acuna, A. and Amat-Guerri, Francisco and Morcillo, Purificacion and Liras, Marta and Rodriguez, Benjamin. Structure and Formation of the Fluorescent Compound of Lignum nephriticum. *ORGANIC LETTERS*, 11(14):3020–3023, JUL 16 2009.

[6] David M. Jameson laboratory in the Department of Cell and Molecular Biology at the John A. Burns School of Medicine of the University of Hawaii on Manoa. `http://thejamesonlab.files.wordpress.com/2011/04/summer-2008c-0441.jpg`, Dec 2013.

[7] Željka Antić, Radenka M. Krsmanović, Marko G. Nikolić, Milena Marinović-Cincović, Miodrag Mitrić, Stefano Polizzi, and Miroslav D. Dramićanin. Multisite luminescence of rare earth doped tio2 anatase nanoparticles. *Materials Chemistry and Physics*, 135(2–3):1064 – 1069, 2012.

[8] T.; Hiltunen L.; Leskela M.; Niinisto L. Tammenmaa, M.; Koskinen. Growth of zinc sulfide thin films using zinc acetate as zinc source and manganese and lanthanoid -diketonates as activator sources. In *Symp. At. Layer Epitaxy, 1st*, 1984.

[9] M. Tammenmaa, T. Koskinen, L. Hiltunen, L. Niinisto, and M. Leskela. Zinc chalcogenide thin films grown by the atomic layer epitaxy technique using zinc acetate as source material. *Thin Solid Films*, 124(2):125 – 128, 1985.

[10] Jaan Aarik, Aleks Aidla, Teet Uustare, and Väino Sammelselg. Morphology and structure of tio2 thin films grown by atomic layer deposition. *Journal of Crystal Growth*, 148(3):268 – 275, 1995.

[11] J. Aarik. Atomic-layer growth of TiO2-II thin films. *Philosophical Magazine Letters*, 73(3):115–119, 1996.

[12] J. Aarik, A. Aidla, H. Mändar, and T. Uustare. Atomic layer deposition of titanium dioxide from ticl4 and h2o: investigation of growth mechanism. *Applied Surface Science*, 172(1–2):148 – 158, 2001.

[13] Per-Anders Hansen, Helmer Fjellvag, Terje Finstad, and Ola Nilsen. Structural and optical properties of lanthanide oxides grown by atomic layer deposition (Ln = Pr, Nd, Sm, Eu, Tb, Dy, Ho, Er, Tm, Yb). *Dalton Trans.*, 42:10778–10785, 2013.

[14] Qingguo Meng, Robert J. Witte, Yajuan Gong, Elizabeth L. Day, Jiangchao Chen, P. Stanley May, and Mary T. Berry. Thin film deposition and photodissociation mechanisms for lanthanide oxide production from tris(2,2,6,6-tetramethyl-3,5-heptanedionato)ln(iii) in laser-assisted mocvd. *Chemistry of Materials*, 22(22):6056–6064, 2010.

[15] Karina Barnholt Klepper, Ola Nilsen, and Helmer Fjellvag. Deposition of thin films of organic-inorganic hybrid materials based on aromatic carboxylic acids by atomic layer deposition. *Dalton Trans.*, 39:11628–11635, 2010.

[16] Karina Barnholt Klepper, Ola Nilsen, Per-Anders Hansen, and Helmer Fjellvag. Atomic layer deposition of organic-inorganic hybrid materials based on saturated linear carboxylic acids. *Dalton Trans.*, 40:4636–4646, 2011.

[17] Damian Wojcieszak, Danuta Kaczmarek, Jaroslaw Domaradzki, Anna Lukowiak, and Wieslaw Strek. Influence of terbium on structure and luminescence of nanocrystalline tio2 thin films. *Central European Journal of Physics*, 11(2):239 –244, 2013.

[18] Danuta Kaczmarek, Jaroslaw Domaradzki, Agnieszka Borkowska, Artur Podhorodecki, Jan Misiewicz, and Karolina Sieradzka. Optical emission from eu, tb, nd luminescence centers in tio2 prepared by magnetron sputtering. *Optica Applicata*, 37:433–438, 2007.

[19] T Suntola and J Hyvarinen. Atomic Layer Epitaxy. *Annual Review Of Materials Science*, 15:177–195, 1985.

[20] Nicola Pinna and Mato Knez. *Atomic Layer Deposition of Nanostructured Materials, Front Matter*. Wiley-VCH Verlag & Co. KGaA, Weinheim, Germany, 1st edition, 2012.

[21] Ingrid Vee. Fluorholdige hybridmaterialer med atomlagsavsetting: Syntese og karakterisering. Master's thesis, Universitetet i Oslo, Norway, 2012.

[22] Hiroyuki Fujiwara. *Spectroscopic Ellipsometry, Prinsiples and Applications*. John Wiley & Sons Ltd, The Atrium, Southern Gate, Chichester, West Sussex Po19 8SQ, England, 2007.

[23] J. Workman and A. Springsteen. *Applied Spectroscopy: A Compact Reference for Practitioners*. Elsevier Science, 1998.

[24] G. Gauglitz and T. Vo-Dinh. *Handbook of Spectroscopy*. Wiley, 2006.

[25] J. Als-Nielsen and D. McMorrow. *Elements of Modern X-ray Physics*. Wiley, 2011.

[26] Consejo Superior de Investigaciones Científicas. Crystallography. `http://www.xtal.iqfr.csic.es/Cristalografia/parte_10-en.html`. 2013-08-18.

[27] Center for Materials and Devices for Information Technology Research Wiki. X-ray diffraction. `http://www.xtal.iqfr.csic.es/Cristalografia/parte_10-en.html`. 2013-10-22.

[28] Wikipedia user:Cdang. `http://upload.wikimedia.org/wikipedia/commons/2/26/Braggs_Law.svg`. 2013-10-22.

[29] B. Beckhoff, B. Kanngie_er, N. Langhoff, R. Wedell, and H. Wolff. *Handbook of Practical X-Ray Fluorescence Analysis*. SpringerLink : Bücher. Springer, 2007.

[30] C.G. Barkla and C.A. Sadler. Lxix. the absorption of röntgen rays. *Philosophical Magazine Series 6*, 17(101):739–760, 1909.

[31] Charles G. Barkla. Xxxix. the spectra of the fluorescent röntgen radiations. *Philosophical Magazine Series 6*, 22(129):396–412, 1911.

[32] N. Bohr. I. on the constitution of atoms and molecules. *Philosophical Magazine Series 6*, 26(151):1–25, 1913.

[33] Thermo Fisher Scientific Inc. Uniquant. `http://www.uniquant.com/introduction.html`. 2014-02-21.

[34] Sheffield Hallam University: Faculty of Health and Wellbeing: Biosciences Division: On-Line Learning. Uv-vis. luminescence spectroscopy - theoretical principles. http://teaching.shu.ac.uk/hwb/chemistry/tutorials/molspec/lumin1.htm. 2014-02-22.

[35] G. Sauerbrey. Verwendung von Schwingquarzen zur Wägung dünner Schichten und zur Mikrowägung. 155:206–222, April 1959. Provided by the SAO/NASA Astrophysics Data System.

[36] Karina Barnholt Klepper. *Deposition of organic-inorganic hybrid materials by atomic layer deposition*. PhD thesis, Universit of Oslo, Norway, April 2011.

[37] Strem Chemicals inc. Product catalog cas number: 15492-51-0. http://www.strem.com/catalog/v/65-8000/71/terbium_15492-51-0. 2014-02-22.

[38] American Chemical Society. Scifinder - cas registry number: 100-21-0. https://scifinder.cas.org/scifinder/view/scifinder/scifinderExplore.jsf. 2014-02-22.

[39] Sigma-Aldrich. Titanium(iv) chloride. http://www.sigmaaldrich.com/catalog/product/sial/254312?lang=en&region=NO. 2014-02-22.

[40] S Quezel-Ambrunaz and E.F Bertaut. Structure magnetique de l'oxyde de terbium tbo2. *Solid State Communications*, 11(5):605 – 610, 1972.

[41] Il'in A.G. Kashaev A.A., Ushchapovskii L.V. Electron-diffraction and x-ray diffraction study of rare earth metal oxides in thin films. *Sov. Phys. Crystallogr. (Engl. Transl.) (1975) 20, 114-115*, 20:114–115, 1975.

[42] Gil'man I.Y. Andreeva A.F. Polymorphic transitions in rare earth oxides obtained by reactive evaporation. *Inorg. Mater.*, 14:384–390, 1978.

[43] J. W. Elam and S. M. George. Growth of zno/al2o3 alloy films using atomic layer deposition techniques. *Chemistry of Materials*, 15(4):1020–1028, 2003.

[44] G. J. McCarthy. Crystal data on *c*-type terbium sesquioxide (Tb_2O_3). *Journal of Applied Crystallography*, 4(5):399–400, Oct 1971.

[45] G. Wakefield, H.A. Keron, P.J. Dobson, and J.L. Hutchison. Structural and optical properties of terbium oxide nanoparticles. *Journal of Physics and Chemistry of Solids*, 60(4):503 – 508, 1999.

[46] Ola Nilsen, Karina Klepper, Heidi Nielsen, and Helmer Fjellvaåg. Deposition of organic- inorganic hybrid materials by atomic layer deposition. *ECS Transactions*, 16(4):3–14, 2008.

A Analysis of noise on QCM signal

There is an extra signal in theQCM data that is causing some difficulty with some of the analysis of the data. Several methods of removing the signal were attempted, but left the data more noisy than before filtering. The signal causes the change in frequency to have an extra uncertainty of about 3 Hz, about 10% of the change due to the mass increase of the $Tb(thd)_3$ pulse and 30% of the 1,4-bdc pulse.

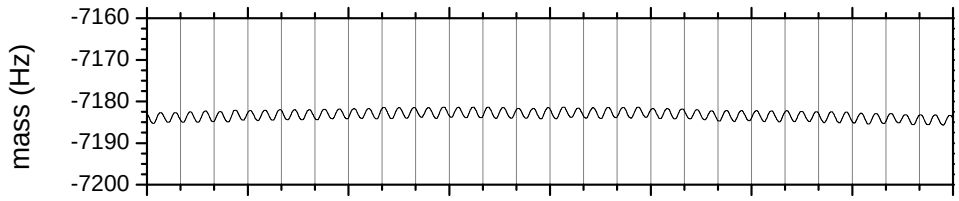

Figure 48: QCM data from the long temperature stabilization phase before the ALD reactions. The space between the grid lines represents 10 seconds.

The oscillations in the QCM data could potentially cause problems for calculations of how much mass reacted on the substrate per cycle. Therefore the change in mass for each cycle was calculated and plotted in figure 49 to evaluate how much of a problem the extra signal is. For the $Tb(thd)_3$ part of the cycle the problem may cause significant uncertainty.

The mean increase in mass for the Tb pulse is -30.98 Hz with a difference of 4.8 between maximum and minimum. This means that the oscillation probably causes an extra 7.75% variation of the mass increase from the mean for the $Tb(thd)_3$ pulse.

For the $Tb(thd)_3$ purge the mean in 1.653 and the difference between maximum and minimum is 2.6Hz. The variation in mass decrease from the mean for the purges is 68.7%.

When considering the total mass increase during pulse and purge of $Tb(thd)_3$ the mean is 29.33Hz with a difference between maximum and minimum of 5.8Hz. The variation in mass increase from the mean for the both pulse and purge together is 9.89%.

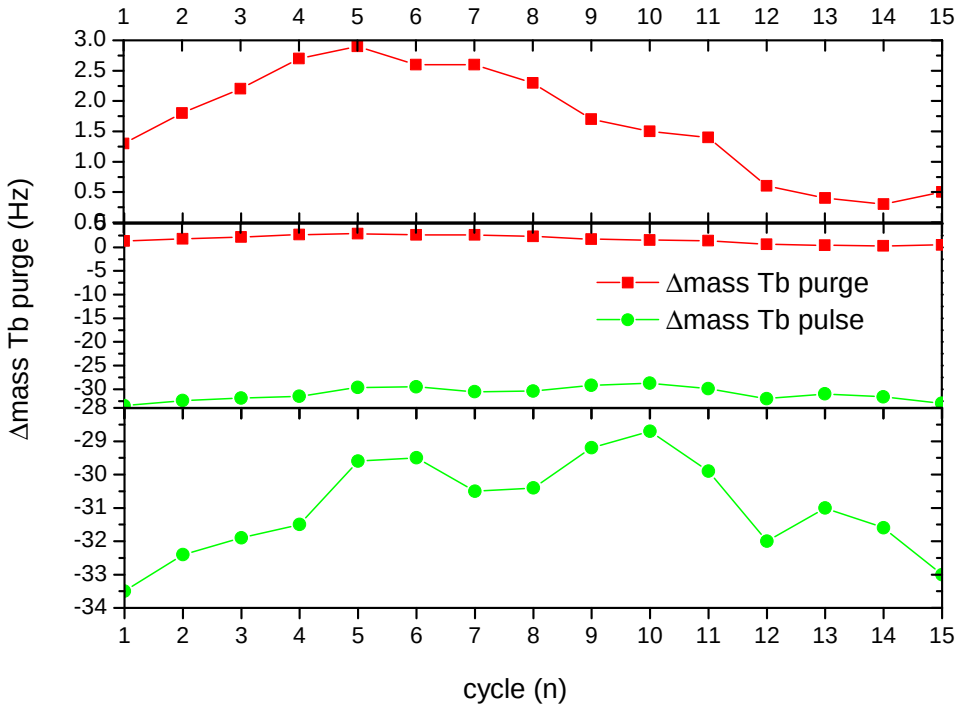

Figure 49: Graphs showing the variations in Δmass per cycle for each cycle in the long cycle phase of the QCM experiment. The top graph shows the change in mass per cycle of only $Tb(thd)_3$ purge and the bottom graph shows change in mass per cycle of only $Tb(thd)_3$ pulse. The middle graph shows both graphs in the same coordinate system to give a sense of scale of the variations. Negative values show increased mass while positive values show decreased mass.

It is easy to see in figure 50 that the oscillations showing in the QCM data for the 1,4-bdc part of the cycles has even larger variation than the $Tb(thd)_3$ part of the cycles. The change in mass during the first second of the 1,4-bdc pulse, the steepest part of the hybrid pulse, is the part that show the lease variation. The mean is 6.94Hz while the difference between maximum and minimum is 2.0Hz, a variation of 14.4%. The total mass decrease during pulse and purge of 1,4-bdc has a mean of 8.44Hz, a variation between maximum and minimum of 5.4 which gives a variation from the mean of 32.0%.

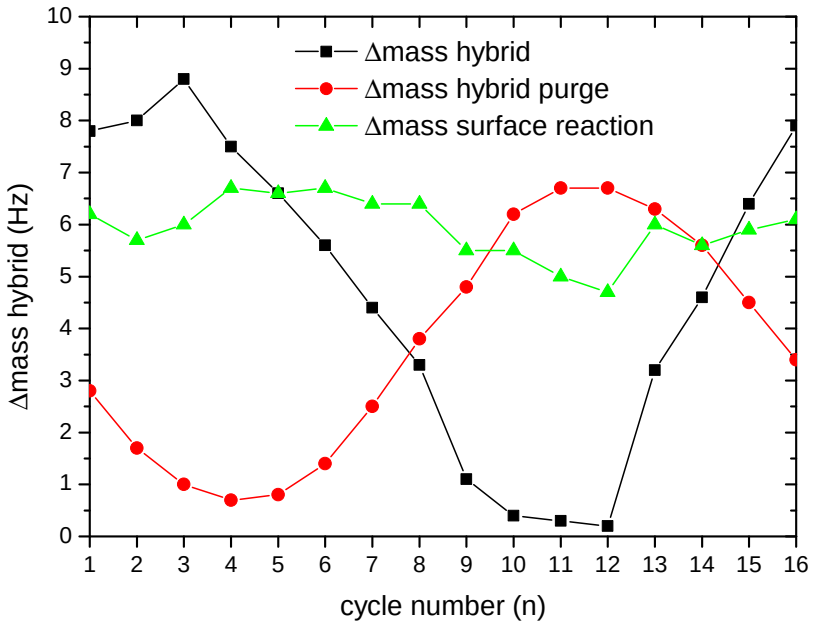

Figure 50: Graph showing the variations in Δmass per cycle for each cycle in the long cycle phase of the QCM experiment. The reaction dataset is the first second of the 1,4-bdc pulse, which is also the part of the 1,4-bdc pulse were the mass is reduced. Negative values show increased mass while positive values show decreased mass.

B Variations in films thickness on a single substrate

The areas attempted measured for the left graph in figure 52 are shown in figure 51. Due to the oblique angle of the light beam on the sample causes the round shape of the incident light beam to reflect on a ellipsoid area. The first digit of the labels denotes which edge was measured and the second digit denotes which area, from left to right, was measured. For example the three areas at the top will be 1-1, 1-2 and 1-3 respectively. The area in the centre is labeled centre.

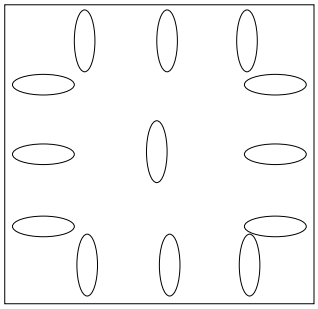

Figure 51: Areas on the sample attempted to measure for figure 52.

In case the slight increase in thickness found in figure 43 are due to slight differences in thickness across the sample two series of ellipsometry measurements were done on the same sample measure for figure 43. When the first series to be measured, on the right in figure 52, the areas measured were not recorded. Instead the sample was shifted slightly in a semi-random fashion to adjust the area of the sample that was measured. The slightly thicker areas measured in the first series seemed to be bunched together, and so a new series was measured where the pattern and area measured was recorded.

The ellipsometry measurements are difficult to limit to a small area of the sample due to the instruments changing the position of the sample while in the process of measuring. When measuring the second series across the same sample the intention was to find a pattern, if any, to where on the substrate the film is thickest. Figure 52 shows no clear pattern for which part of the sample is thickest.

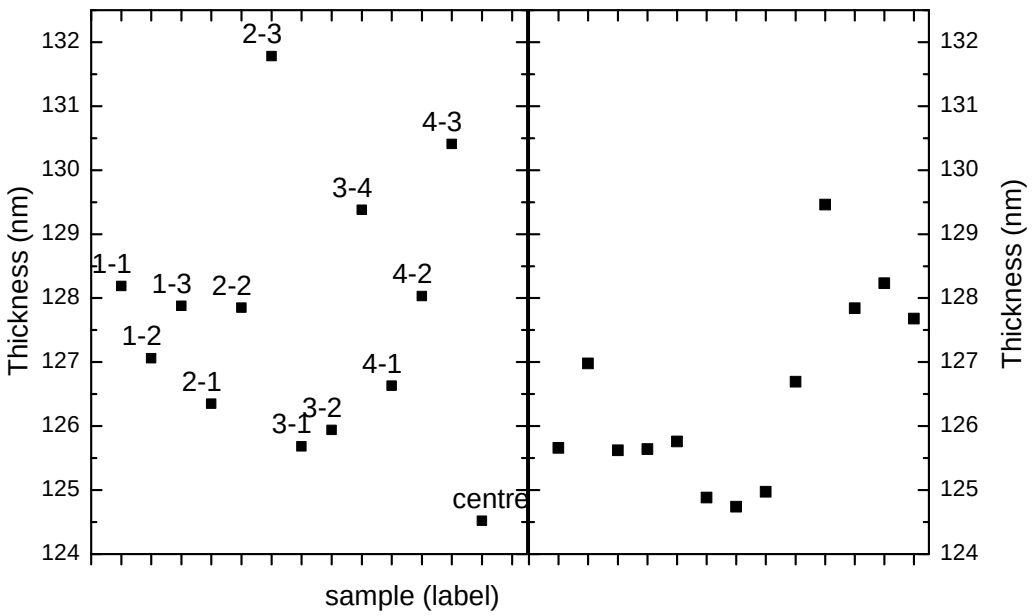

Figure 52: Graph showing thickness measurements on different areas of the same sample. The measurements on the left graph are taken at a later time than those on the right graph. In order to record which area of the substrate was measured the measurements were redone resulting in the graph on the left.